

1       **Airborne bacteria viability and air quality: a protocol to quantitatively investigate the**  
2                               **possible correlation by an atmospheric simulation chamber**

3  
4       *Virginia Vernocchi*<sup>1</sup>, *Elena Abd El*<sup>1,2</sup>, *Marco Brunoldi*<sup>1,2</sup>, *Silvia Giulia Danelli*<sup>1</sup>, *Elena Gatta*<sup>2</sup>,  
5       *Tommaso Isolabella*<sup>1,2</sup>, *Federico Mazzei*<sup>1,2\*</sup>, *Franco Parodi*<sup>1</sup>, *Paolo Prati*<sup>1,2</sup>, *Dario Massabò*<sup>1,2</sup>

6  
7       <sup>1</sup> INFN, Sezione di Genova, via Dodecaneso 33, 16146 Genova, Italy

8       <sup>2</sup> Dipartimento di Fisica, Università di Genova, via Dodecaneso 33, 16146 Genova, Italy

9  
10       *Keywords:* measure technique for bioaerosol, airborne bacteria, Atmospheric Simulation  
11       Chambers.

12       \* *Corresponding author:* Federico Mazzei; federico.mazzei@ge.infn.it

13  
14                               **Abstracts**

15       Biological Particulate Matter or bioaerosol are a subset of atmospheric aerosol. They influence  
16       climate, air quality and health via several mechanisms which often are poorly understood. In  
17       particular, the quantitative study of possible relationship between bioaerosol viability and air  
18       quality or meteorological conditions is an open and relevant issue. The difficulty of retrieving such  
19       possible correlations by analyses of data collected during in-field campaigns, can benefit of  
20       targeted experiments conducted in well controlled conditions inside Atmospheric Simulation  
21       Chambers, ASCs. ChAMBRe (Chamber for Aerosol Modelling and Bio-aerosol Research) is an  
22       ASC in Genoa (Italy) designed and built to perform experimental research on bioaerosol. In this  
23       article we focus on bacteria viability. A multi-step protocol was developed and thoroughly tested:  
24       cultivation of a suitable bacteria population (*E. coli*), nebulization and injection in the chamber of  
25       viable cells, exposure and monitoring of the viability variation inside ChAMBRe, hold at selected  
26       conditions, and finally incubation and counting of the concentration of viable bacteria. The whole  
27       procedure showed an estimated lifetime of total (T) and viable (V) *E. coli* of about 153 and 32  
28       minutes, respectively, and a V:T ratio lifetime of  $40 \pm 5$  minutes when ChAMBRe is held in a  
29       reference “baseline” condition. The coefficient of variation of 13% shows how sensitive the  
30       protocol is also to changes in viability when the bacteria are exposed to other (e.g., polluted)  
31       conditions. First results showing a viability reduction observed exposing the *E. coli* strain to NO<sub>x</sub>

32 concentrations and solar irradiation are presented and discussed. Present results pave the way to  
33 systematic studies aimed at the definition of dose-effect relationship for several bacteria strain at  
34 atmospheric pollutants.

35

## 36 **1. Introduction**

37 This article focusses on *bioaerosol*, the aerosol of biological origin. The major types of bioaerosols  
38 are primary and secondary biological aerosols and biogenic aerosols.

39 Primary biological aerosols (PBAs) refer to bioaerosols that are directly released into the  
40 atmosphere from biological sources, such as plants, animals, or microorganisms; these aerosols  
41 can be composed of various biological materials, including bacteria, viruses, fungi, pollen, spores,  
42 algae, or other organic particles (Ariya and Amyot, 2004; Fröhlich-Nowoisky et al., 2016).

43 Secondary biological aerosols (SBA) are the result of environmental processes or human activities  
44 that modify or transform primary biological aerosols. Unlike primary biological aerosols, SBA are  
45 not directly released from biological sources but are generated through secondary processes, like  
46 oxidation, condensation, etc., involving biological materials. SBA are fragments of larger  
47 biological particles, material released from cells (disruption, excretion...), nucleated biogenic  
48 gases, or cells “born” in the air from microbial multiplication (Morris et al., 2014, Ervens et Amato,  
49 2020).

50 The PBAs vary in size depending on the specific biological material being aerosolized; they range  
51 from several nanometers (e.g., viruses, cell fragments) to a few hundred micrometers in  
52 aerodynamic diameter (e.g., pollen, plant debris) (Pöschl, 2005). Larger particles of biological  
53 material, such as large pollen grains or larger fragments of plants or insects, can be lifted into the  
54 air; however, due to their relatively high settling velocities, they tend to rapidly settle or deposit  
55 onto surfaces rather than remain suspended in the air for extended periods. As a result, these larger  
56 particles are typically not considered atmospheric aerosol particles (Després et al., 2012).

57 Among all the different bioaerosol microorganisms, bacteria are considered to play a significant  
58 role in the composition and dynamics of bioaerosols (Gong et al., 2020). They are ubiquitous in  
59 the atmosphere, and their presence and abundance can vary depending on factors such as location,  
60 season, and local environmental conditions: usually, over the land, the concentration in atmosphere  
61 is greater than  $10^4$  cells  $m^{-3}$  (Burrows et al., 2009) while our understanding of airborne microbes  
62 over oceans, is indeed limited compared to the knowledge we have about microbes in terrestrial

63 and aquatic environments. In a recent work (Mayol et al., 2014), the airborne prokaryotic  
64 abundance over the North Atlantic Ocean ranged from about 3000 to 20000 prokaryotes  $\text{m}^{-3}$   
65 (average about 8000 cells  $\text{m}^{-3}$ ).

66 Bacteria, as small airborne particles, or aerosols can have relatively long atmospheric residence  
67 times compared to larger particles. This is due to their small size and low settling velocity, which  
68 allows them to remain suspended in the air for prolonged periods. (Després et al., 2012). Airborne  
69 bacteria may be suspended as individual cells or attached to other particles, such as soil or leaf  
70 fragments, or found as agglomerates of many bacterial cells (Lighthart et al., 1993). For this reason,  
71 whereas individual bacteria are typically on the order of  $\sim 1 \mu\text{m}$  or less in size, the median  
72 aerodynamic diameter of particles containing culturable bacteria at several continental sites has  
73 been reported to be  $\sim 2 - 4 \mu\text{m}$  (Shaffer and Lighthart, 1997; Wang et al., 2007). Even if up to now  
74 several works have contributed to the identification of bacterial diversity in the atmosphere (Amato  
75 et al., 2007; Burrows et al., 2009; Després et al., 2012, Romano et al., 2019), it remains difficult  
76 to establish a clear picture of the actual abundance and composition of bacteria in the air.  
77 Numerous studies have suggested that the presence of bacteria in the atmosphere can have  
78 significant implications for cloud formation, atmospheric chemistry, microbial biogeography, and  
79 climate. As a matter of fact, bacteria can serve as ice nucleating particles and cloud condensation  
80 nuclei, influencing the precipitation processes, affecting cloud lifetime, optical properties, and  
81 climate patterns (Bauer et al., 2003; Morris et al., 2004; Sun and Ariya, 2006; Möhler et al., 2007).  
82 In particular, bacterial viability, the proportion of viable to total bacteria concentration, can act as  
83 Cloud Condensation Nuclei (CCN) thanks to the hygroscopic properties of their surfaces (Delort  
84 et al., 2010). Additionally, the near-surface atmosphere's viable bacteria can have a significant  
85 impact on human health, including allergies, acute toxic effects, and infections (Bolashikov and  
86 Melikov 2009).

87 Since bacteria have also been shown to metabolize within cloud droplets, some authors have  
88 proposed an impact on the chemistry of cloud droplets and air (Fankhauser et al., 2019; Jaber et  
89 al., 2020, 2021; Khaled et al., 2021). Finally, the presence of bacteria in the atmosphere can  
90 influence microbial biogeography (Martiny et al., 2006) by facilitating long-distance dispersal and  
91 the establishment of microbial populations in new environments.

92 Bacteria can enter the atmosphere as aerosol particles from various surfaces, including soil, water,  
93 and plant surfaces (Burrows et al., 2009). Once in the air, they are carried upwards by air currents

94 and may remain in the atmosphere for many days before being removed by wet or dry deposition  
95 onto surfaces. Indeed, the mechanisms that govern the transport, survival, and activity of bacteria  
96 in the atmosphere are complex and multifaceted. Understanding these mechanisms is crucial for  
97 various scientific disciplines, including microbiology, atmospheric science, and public health. This  
98 complexity is related to some key factors such as aerosolization, transport and dispersion, survival,  
99 hygroscopicity, interactions with other particles, droplet nucleation, deposition, activation of ice  
100 nucleation, impacts on cloud formation and chemistry and all these processes are indeed  
101 intertwined (Amato et al., 2023). The interactions between bacteria and their living environment,  
102 as well as the atmospheric conditions, play crucial roles in determining their behavior and impacts  
103 on climate (Deguillaume et al., 2008) and, consequently, on health.

104 Atmospheric Simulation Chambers (ASCs) have been widely used to study chemical and  
105 photochemical atmospheric processes, but the high versatility of these facilities allows for a wider  
106 application covering all fields of atmospheric aerosol science. For example, a consistent  
107 improvement in characterizing bioaerosols, in understanding the mechanisms affecting their  
108 behavior in the atmosphere and finally in elucidating their impacts, can be obtained using  
109 atmospheric chamber facilities, where transdisciplinary studies addressing atmospheric physics,  
110 chemistry, and biology issues are possible.

111 In the last decades, the use of atmospheric simulation chambers has been much more focused on  
112 the potential interest of bioaerosol as ice nuclei and cloud condensation activity (Bundke et al.,  
113 2010; Chou, 2011). Few studies have investigated bacterial survival and activity using simulation  
114 chambers, and some of them are old (Wright et al., 1969 Ehrlich et al., 1970; Krumins et al., 2014).  
115 Recently, addressing the public health concerns related to bioaerosol contamination has led to  
116 increased research efforts focusing on the survival and transformation of bioaerosols in the  
117 atmospheric environment. Innovative chamber studies have been initiated to investigate these  
118 questions and gain insights into the behavior of bioaerosols (Amato et al., 2015; Brotto et al.,  
119 2015). These works have led to the development of a new dedicated simulation chamber,  
120 ChAMBRe (Massabò et al., 2018). The chamber has been installed at the National Institute of  
121 Nuclear Physics in Genoa (IT) in collaboration with the Environmental Physics Laboratory at the  
122 Physics Department of the University of Genoa. ChAMBRe is also a National Facility of the  
123 constituting ERIC-ACTRIS, the worldwide largest research infrastructure to study atmospheric  
124 phenomena, set up by the European Union on April 25<sup>th</sup> 2023 (CID, 2023). The main scientific

125 target at ChAMBRé, is the description of biological micro-organisms behavior in the atmosphere,  
126 aiming to a deeper understanding of the still unclear mechanisms that control the evolution of  
127 bioaerosols in atmosphere, in particular their bacterial components. The long-term goal is the  
128 parameterization of survival and activity of bioaerosols to develop specific tools to be implemented  
129 in chemical transport models (e.g., CAMx, Wagstrom et al., 2008) presently limited to treat  
130 transport and chemistry of gaseous and not-biological aerosol species.

131 This article gives all the details of the present status and capability of the ChAMBRé facility and  
132 introduces a multi-step, interdisciplinary procedure assessed to perform quantitative studies on the  
133 impact of different pollutants on bacteria viability. Preliminary results are also shown to illustrate  
134 the sensitivity of the experimental procedures developed at ChAMBRé that pave the road to  
135 systematic investigations on different strains and air quality conditions.

136

## 137 **2. Material and Methods**

138 Since the beginning of 2017, ChAMBRé has been one of the nodes of the EUROCHAMP-2020  
139 network with specific tasks on bio-aerosol studies. From the date of installation, on ChAMBRé  
140 control and acquisition system has been enriched with a wide range of equipment aimed at  
141 monitoring and controlling the processes occurring inside the chamber. In addition, most efforts  
142 have been devoted to developing protocols to produce, inject, expose, and collect bio-aerosols, to  
143 maximize the experiments reproducibility.

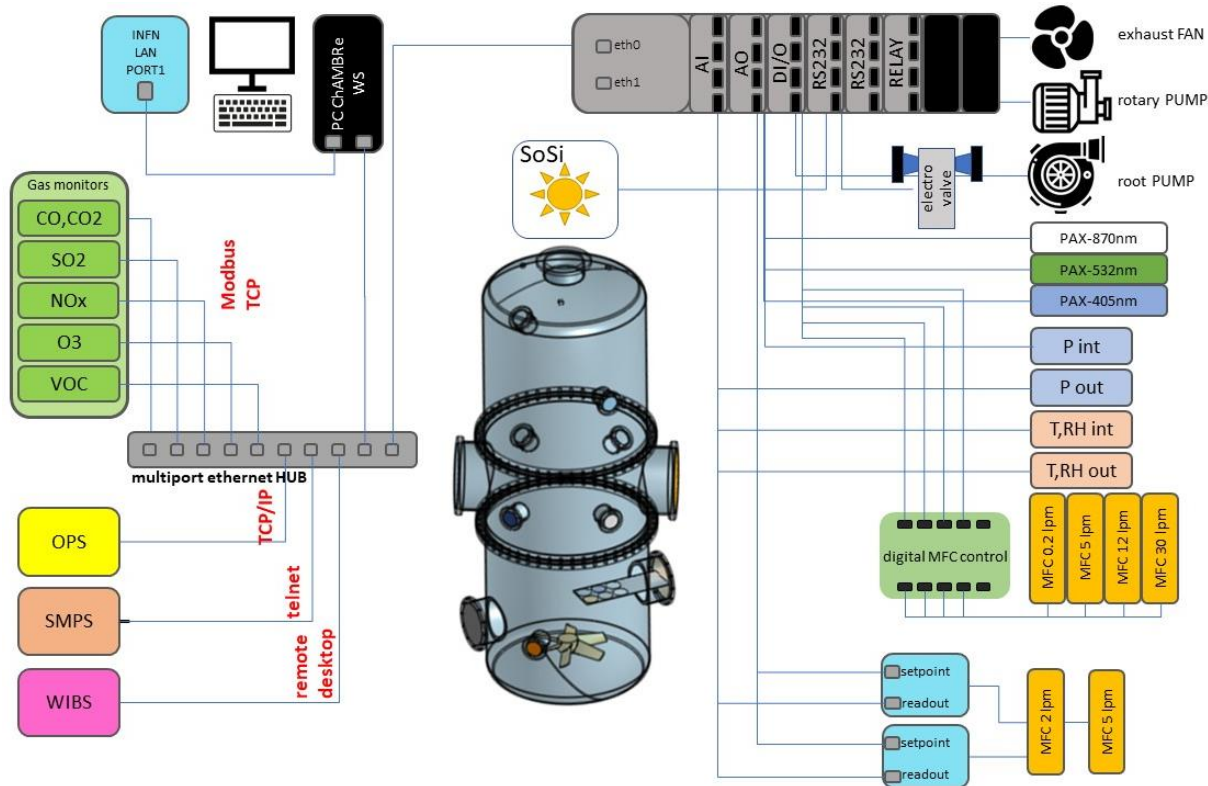


Figure 1: ChAMBRe layout

144

145

146

147 Briefly, ChAMBRe (Massabò et al., 2018) has a cylindrical shape with domed bases. It has a  
 148 maximum height and diameter of 2.9 and 1 m, respectively, and a total volume of about 2.2 m<sup>3</sup>.

149 The main body is divided into three parts (two domed cylinders connected by a central ring)  
 150 equipped with several flanged apertures of different diameters matching the different types of  
 151 fitting for instrument interfacing.

152 To favor the mixing of the gas and aerosol species, a fan is installed at the bottom of the chamber.  
 153 It is a standard venting system with a particular pass-through designed and built at INFN-Genoa  
 154 to ensure the vacuum seal. The fan speed can be regulated by an external controller and set up to  
 155 50 Hz in steps of 0.1 Hz.

156 One of the two flanges in the bottom part is connected through a pneumatic valve to a smaller  
 157 horizontal cylinder (length about 1 m), which hosts a movable tray designed to move specific  
 158 samples inside the chamber. The samples are typically Petri-dishes for bacteria collection inside  
 159 the chamber during the experiments: they can remain exposed for the whole experiment or for a  
 160 selected time interval controlled by the user. A custom-made side flange has been worked in the  
 161 central ring of the main body of the chamber. The large tipper tailgate allows the introduction and

162 positioning of bulky sensor devices for testing and calibration purposes. The flange features a  
163 small window for visual inspection and four vacuum feedthrough connectors to power and  
164 communicate with devices inserted in the chamber.

165 ChAMBRé is equipped with a composite pumping system (rotary, root and turbo pump) which  
166 can evacuate the internal volume to a level of about  $5 \times 10^{-4}$  mbar. The return to atmospheric  
167 pressure can proceed by flowing ambient air inside the chamber through a five-stage  
168 filtering/purifying/drying inlet system including an absolute HEPA filter and a zeolite trap or using  
169 synthetic air from a cylinder (reducing the relative humidity close to zero).

170 Two types of UV lamps are permanently installed inside the chamber. A 58 cm long lamp ( $W =$   
171  $60$  W,  $\lambda = 253.7$  nm; UV-STYLO-F-60H, Light Progress Srl) is inserted through a custom side  
172 flange to sterilize the chamber volume without producing ozone after any experiment involving  
173 bioaerosol. A second type of lamp, producing UV radiation at  $\lambda < 240$  nm, can be inserted through  
174 one of the ISOK100 flanges of the central ring to generate ozone.

175 A set of two pressure gauges is used to measure the atmospheric pressure inside (range  $5 \times 10^{-4}$  -  
176  $10^3$  mbar) and outside (range of  $5 \times 10^{-2}$  -  $10^3$  mbar). ChAMBRé internal temperature and relative  
177 humidity are continuously measured by a sensor located in the upper ISO-K100 flange on the top  
178 dome.

179 Supervised injection of known volumes of different gas species inside the chamber is made by a  
180 set of software-controlled digital mass flow controllers (MFC) ranging from 5 to 30 lpm full-scale  
181 manufactured by Bronkhorst<sup>®</sup>. Two 5-lpm MFCs are designed for injection of CO<sub>2</sub> and other gases  
182 (i.e. SO<sub>2</sub>, CO, NO and NO<sub>2</sub>), respectively, whose concentration in the chamber can be selected by  
183 the operator (ppm or ppb units); a PID (Proportional–Integral–Derivative) controller, using the gas  
184 concentration values read from the corresponding gas analyser, keeps the gas concentration in  
185 ChAMBRé constant during the experiment.

186 A 30-lpm MFC regulates the injection of dry air inside the chamber. In this case, the PID controller  
187 (using the ChAMBRé pressure values measured by pressure sensor mentioned above) allows to  
188 maintain a pre-defined pressure gap between inside and outside the chamber. A 12-lpm and a 0.2-  
189 lpm MFCs are dedicated to the injection of known volumes of air and fuel, respectively, inside the  
190 burning chamber of a Mini Inverted Soot Generator (Argonaut Scientific Corp., Edmonton, 49  
191 AB, Canada, Model MISG–2). The MISG can be connected to an inlet flange of ChAMBRé for  
192 the study of the properties of soot particles exposed and maintained in different conditions or to

193 study the effects of soot particles. The input air flow of the nebulizers (see Par. 2.2), responsible  
194 for the crucial process of bacteria injection inside the chamber, is regulated by an analog 5-lpm  
195 full-scale MFC (EL-Flow®).

196

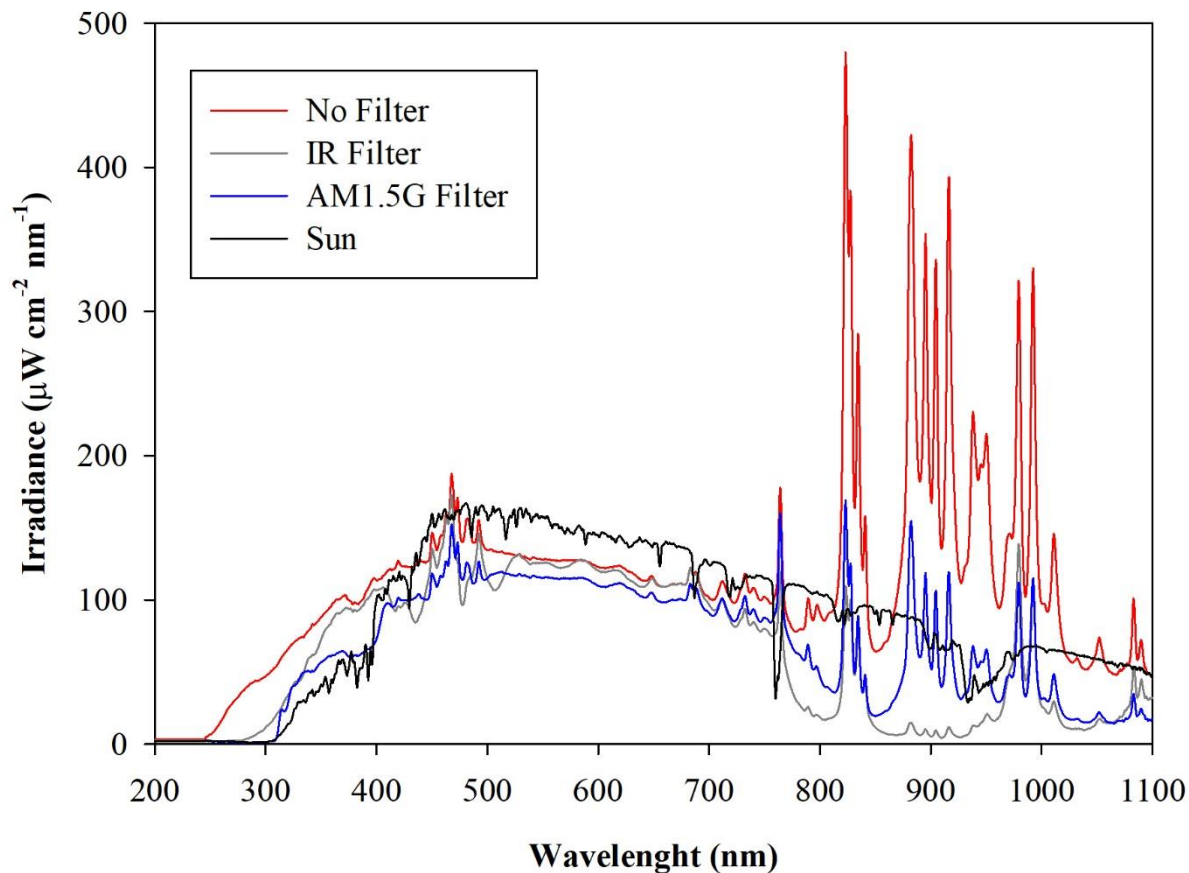
### 197 *2.1 Instruments permanently connected to the chamber.*

198 The concentration of several gaseous pollutants potentially present inside the chamber can be  
199 monitored by a set of calibrated gas detectors manufactured by ENVEA®: non-dispersive Carbon  
200 monoxide and dioxide analyzer (CO12e), Ozone analyzer (O342e), Sulfur dioxide analyzer  
201 (AF22e), chemiluminescent Nitrogen Oxides analyzer (AC32e) and Gas chromatography VOC  
202 analyzer (VOC72M). Details on the quoted monitors are provided in Supplement S1.

203 A custom solar simulator manufactured by Sciencetech™ has been installed on the top of the upper  
204 dome of the chamber. The top ISO-K250 flanged aperture has been appropriately modified by  
205 inserting a dedicated quartz window (diameter = 25 cm) with a high degree of transmittance (> 95  
206 %, with  $300 < \lambda < 900$  nm) and reflectance (< 1.5% with  $300 < \lambda < 900$  nm) to the solar spectrum  
207 radiation. The system consists of two main sections: the light source and the power supply. The  
208 light source, a 1600 W Xenon Short Arc lamp (Sciencetech™ - XE1600), is mounted inside a  
209 dedicated housing where a set of optical lenses and mirrors deflects the light beam perpendicularly  
210 to fit the quartz window aperture. A set of filters are available to intercept the light beam and cut-  
211 off selectable portions of the spectrum before entering the chamber. In particular, the simulator  
212 can be fitted with a low-pass optical filter, designed to cut off a portion of the spectrum in the  
213 infrared (IR) region. Alternatively, the optical absorption of the atmosphere can be simulated by  
214 using a dedicated filter (AM1.5G  $3 \times 3$ " air mass filter, Sciencetech™), which cuts off selected  
215 bands to mimic the light interaction of an air mass coefficient of 1.5 (i.e., an optical path length  
216 that is 1.5 times that of light traversing the atmosphere at the zenith). Figure 1 shows the impact  
217 of the available filters on the light spectrum sent to the chamber. The nominal maximum irradiance  
218 provided by the Solar Simulator without any filter is about 2.4 SUN, actually  $2,424 \text{ W m}^{-2}$ ,  
219 corresponding to about 119 W passing through the quartz window on the ChAMBRé top dome  
220 with the AM1.5 filter mounted inside the solar simulator.

221



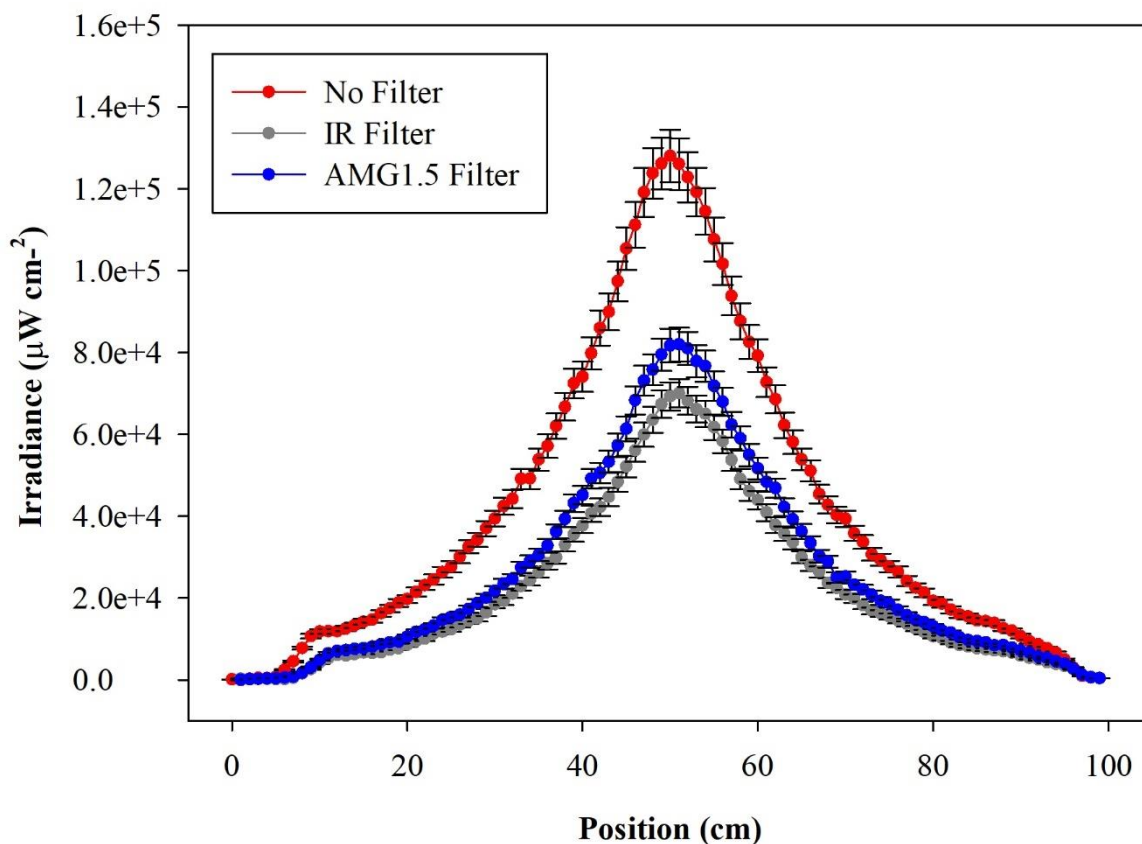


222  
 223 **Figure 2:** Irradiance vs wavelength measured with a calibrated Avantes ULS2048CL-EVO spectrometer directly at  
 224 the exit of the Solar Simulator with and without the available filters. The spectrum labelled “Sun” has been measured  
 225 on a springtime sunny day in the terrace of the Physics Department in Genoa, Italy. The uncertainties of irradiance  
 226 (not reported in the graph) are  $\pm 10\%$  from 200 to 350 nm and 5% from 350 to 1100 nm.

227  
 228 The solar simulator is also equipped with a set of four neutral density optical filters, to reduce the  
 229 light intensity entering the chamber. These filters provide an attenuation of 19%, 34%, 50% and  
 230 71% of the lamp power, respectively, and can be fitted two at a time on the device, offering a  
 231 minimum transmittance of 7%. The neutral density filters do not significantly alter the shape of  
 232 spectrum of the transmitted light, attenuating the optical power uniformly (see Supplement S2,  
 233 Figure S2).

234 The radial distribution of the optical power measured inside the chamber volume is shown in  
 235 Figure 3, as a function of the distance along a cross-sectional diameter in the center of ChAMBRe.  
 236 The light intensity has a strong peak at the center of the diameter, where the optical power is more

237 than six times that close to the walls. To obtain the total light intensity irradiated by the lamp in  
 238 the chamber volume, the measured data points were fitted with a double gaussian function, which  
 239 was then integrated in cylindrical coordinates, exploiting the symmetry of the light beam. The  
 240 resulting intensity is  $160 \pm 6$  W with the lamp set at full power (power supply set at 105% of the  
 241 nominal value) and no optical filter. The total intensity with the AM1.5 filter is  $94 \pm 4$  W, while  
 242 with the IR filter the total integrated intensity is  $81 \pm 4$  W. With respect to the irradiance measured  
 243 directly at the Solar Simulator output, the value inside the chamber shows just a loss of about 20%  
 244 (likely due focusing/collimation). It must be noted that, at the maximum power and no-filter, the  
 245 irradiance measured on the middle plane of ChAMBRe is about 0.2 SUN, this almost  
 246 corresponding to the dilution given by the ratio of the surfaces of the top quartz window (diameter  
 247 of 25 cm) and of the chamber (diameter of 100 cm).



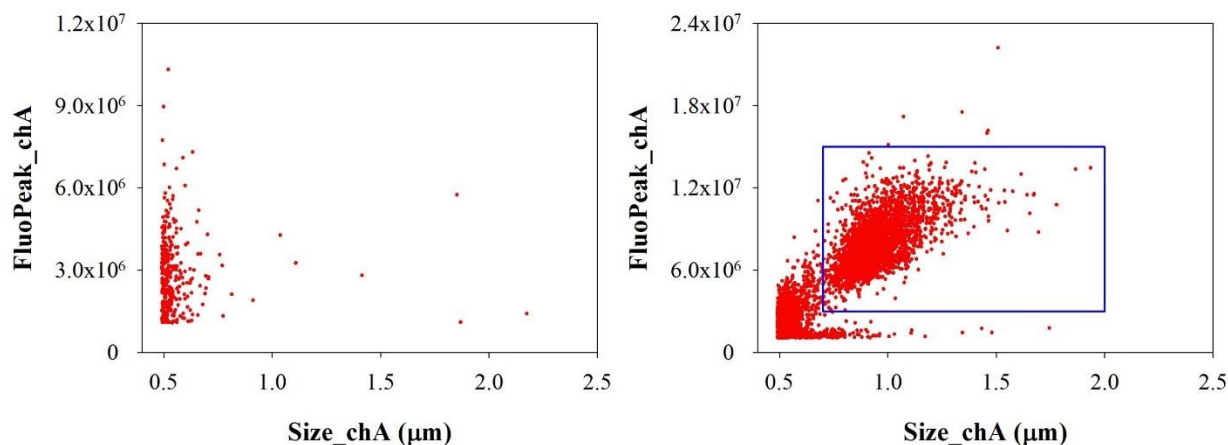
248  
 249 **Figure 3:** Irradiance vs wavelength measured with a calibrated Avantes ULS2048CL-EVO spectrometer along a  
 250 diameter at the center of the ChAMBRe volume, with and without the available optical filters. The center of the  
 251 chamber is at position=50 cm.

252 Particle concentration and size distribution inside ChAMBRe are real-time monitored by a  
253 Scanning Mobility Particle Sizer (SMPS; TSI Inc., model 3938), in the range of 10 – 1000 nm,  
254 and an Optical Particle Sizer (OPS; TSI Inc.; model 3330) in the range 0.3 - 10  $\mu\text{m}$ .  
255 The SMPS is formed by three components: a neutralizer (i.e., a bipolar diffusion charger), a  
256 differential mobility analyzer (DMA, series 3080) and a condensation particle counter (W-CPC,  
257 model 3789), from TSI Inc. The model 3088 Neutralizer uses a low-energy ( $< 9.5\text{keV}$ ) soft X-ray  
258 source to generate high concentrations of both positive and negative ions to bring the aerosol to a  
259 defined, steady-state charge distribution. The DMA is available with two different columns: model  
260 3081 Long DMA, which provides the widest size range of 10-1000 nm, and the model 3085 Nano  
261 DMA, which covers the range of particle diameter from 2 and 150 nm. In a DMA, an electric field  
262 is created and the airborne particles drift in the DMA according to their electrical mobility. Particle  
263 size is then calculated from the mobility distribution. In the CPC, downstream of the DMA, the  
264 particle size is increased by water condensation on their surface and then the particles are optically  
265 counted. The maximum measurable concentration can reach  $2 \times 10^5$  particles  $\text{cm}^{-3}$ . The SMPS  
266 working airflow ranges between 0.2 and 1.5 lpm.

267 The Model 3330 OPS is an optical particle sizer spectrometer that provides measurement of  
268 particle number concentration and particle size distribution based on single particle counting  
269 technology. The OPS has an inlet flow rate of  $1.0 \text{ lpm} \pm 5\%$  and measures particles from 0.3  $\mu\text{m}$   
270 to 10  $\mu\text{m}$  in 16 user-adjustable size channels (particles above 10  $\mu\text{m}$  are counted but not sized).  
271 The OPS 3330 works on the principle of optical scattering from single particles. The OPS uses a  
272 laser beam ( $\lambda = 660 \text{ nm}$ ) and a detector to detect particles passing through a sensing volume  
273 illuminated by the laser. Particle pulses are counted individually and binned into 16 channels up  
274 to their pulse heights. The OPS is factory calibrated using different monodispersed Polystyrene  
275 Latex particles (PSL) for size classification; size resolution is 5% at 0.5  $\mu\text{m}$  following the  
276 procedure described in the ISO 21501-1 normative. Particles exiting the chamber are trapped by a  
277 gravimetric filter for possible after sampling chemical analysis.

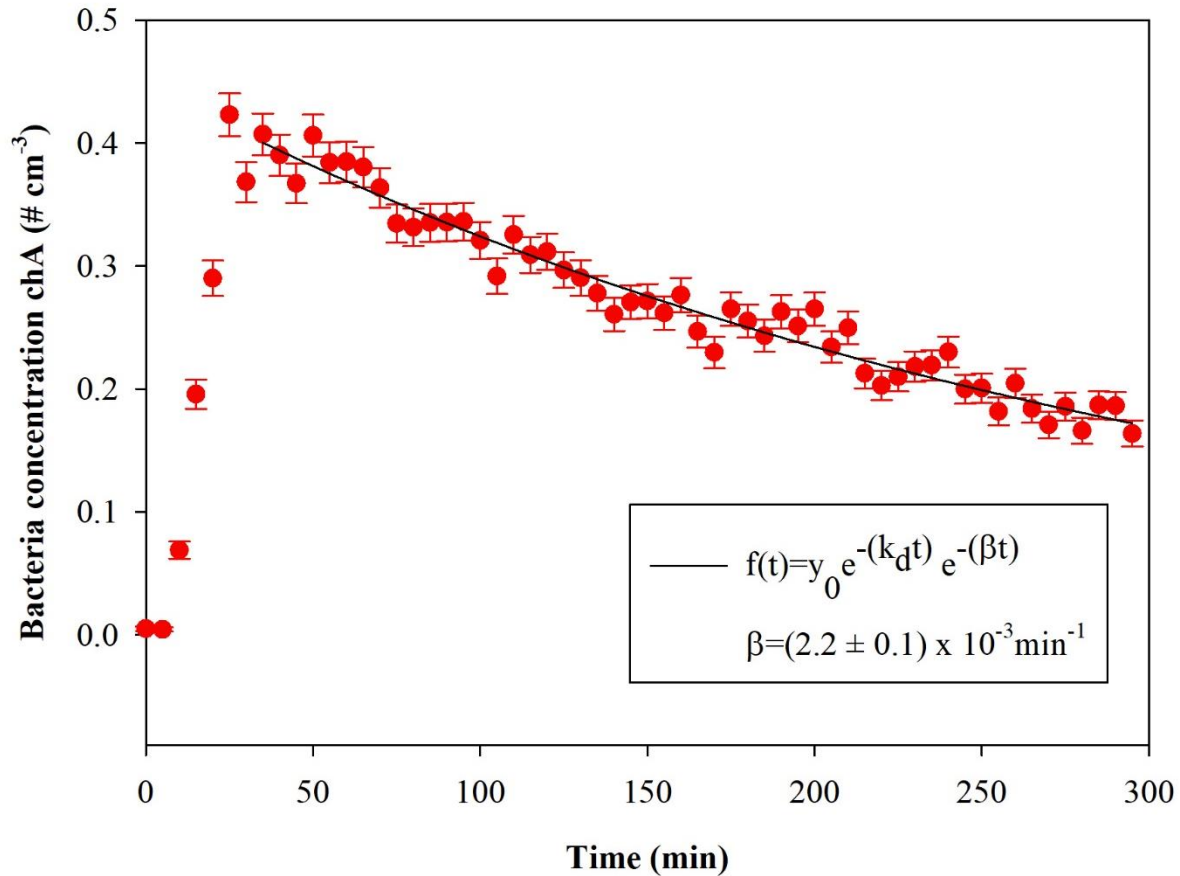
278 A Waveband Integrated Bioaerosol Sensor (WIBS-NEO, Droplet Measurement Technologies<sup>®</sup>)  
279 has been integrated in the ChAMBRe particle monitoring system to measure bio-aerosols  
280 concentration. The instrument uses two UV filtered flashlamp sources ( $\lambda = 280 \text{ nm}$  and  $\lambda = 370$   
281 nm) to excite fluorescence in individual particles (Lieberherr et al., 2021). Detection wavebands

282 have been selected to optimize detection of common bioaerosol components and let the user  
283 discriminate between different types of biological micro-organisms (bacteria, fungi, pollen, etc.).  
284 The massive amount of data generated by the WIBS during the experiments at ChAMBRé through  
285 a list-mode off-line analysis, has made necessary to develop a dedicated software tool, written in  
286 Igor 8.0 (Wavemetrics, Inc.) language, aimed at implementing a multi-parametric data reduction  
287 and to retrieve the airborne bacteria/bioaerosol concentration inside the chamber as a function of  
288 time. Starting from the raw data, the Igor procedure first sets a background threshold for the  
289 particle fluorescence intensity and groups the particles into three channels (A, B, C) and their  
290 relative intersections (AB, AC, BC, ABC) according to their presence within the three fluorescence  
291 detection waveband groups (FL1, FL2, FL3), following the terminology adopted in the WIBS  
292 (Lieberherr et al., 2021). Then, for signal-background separation purpose, fiducial cuts are applied  
293 on scatter plots (Fluorescence Intensity vs Particle Size) relative to particles belonging to channel  
294 A, which is known to be mainly populated by particles showing a bacteria-like fluorescence  
295 emission. Examples of the scatter plots are reported in Figure 4 where the region of interest of the  
296 signal (*E. coli* bacteria) is well separated from the background region.



297  
298 **Fig 4:** Size distribution of particles in channel A. Left: background measured without any bacteria injected in  
299 ChAMBRé. Right: particles population after *E. coli* injection. The particles inside the blue rectangular region of  
300 interest are identified as *E. coli*.

301  
302 Finally, the whole analysis is cycled over user-selectable time intervals to retrieve the time-  
303 resolved particle concentration during the whole experiment. Figure 5 shows the time series of *E.*  
304 *coli* concentration inside the chamber during a typical experiment.



305  
 306 **Figure 5:** Temporal trend of *E. coli* particles inside the chamber;  $t = 0$  is the injection start. The curve fit is also shown,  
 307 where  $\beta$  is the particle loss rate coefficient and  $k_d$  is the dilution factor (here  $k_d = 1.02 \times 10^{-3} \text{ min}^{-1}$ ). The error bars are  
 308 the standard deviations calculated following the Poisson statistics.

309  
 310 Optical properties (i.e., absorption, extinction and scattering coefficients) of particles suspended  
 311 inside the chamber can be measured online by photoacoustic extinction meters (PAXs; Droplet  
 312 Measurement Technologies) at three wavelengths:  $\lambda = 870, 532$  and  $405 \text{ nm}$ .  
 313 The PAX directly measures in-situ light absorption and scattering of aerosol particles, from which  
 314 it derives extinction, single scattering albedo and black carbon mass concentration (Vernocchi et  
 315 al., 2022). PAX uses a modulated diode laser to simultaneously measure light scattering and  
 316 absorption. The standard infrared,  $870 \text{ nm}$  wavelength option, is highly specific to black carbon  
 317 particles, since there is relatively little absorption from gases and non-BC aerosol species at this  
 318 wavelength. A nominal  $1 \text{ lpm}$  aerosol sample flow is drawn into the PAX using an internal vacuum  
 319 pump controlled by two critical orifices. The flow is split between the two distinct measurement  
 320 regions: a nephelometer, for the light scattering measurement and a photoacoustic resonator for

321 the absorption measurement. Absorbing particles heat up and quickly transfer heat to the  
322 surrounding air. A sensitive microphone detects the pressure waves produced by the heating,  
323 whose intensities are interpreted to infer the particle absorption coefficient (Moosmüller et al.,  
324 2009). In the nephelometer, a photodiode set at 90° with respect to the beam detects the radiation  
325 reflected by the sampled particles. The scattering measurement responds to all particle types  
326 regardless of chemical makeup, mixing state, or morphology.

327 Acquisition and control of the instruments connected to ChAMBRé is handled by a National  
328 Instruments™ based system made up of a main controller (NI9057 cRIO) and several modules (C  
329 Series modules), which allow communication with the peripheral devices via analog, serial, and  
330 ethernet data transfer protocols. The operator interaction with the sensor network is demanded to  
331 a single NI-LabVIEW™ SCADA (Supervisory Control And Data Acquisition) custom application  
332 which provides the user with a global data overview and a full real-time control above all the  
333 instruments parameters via a user-friendly human-machine interface (HMI). In Supplement S1  
334 (Figure S1), a screenshot of the main panel of the SCADA application is shown.

335

## 336 *2.2 Other equipment for specific applications/experiments*

337 Aerosols to be used in ChAMBRé experiments can be generated in different ways, depending on  
338 the specific application. The Flow-Focusing Monodisperse Aerosol Generator (FMAG, TSI Inc.  
339 model 1520) can be used to produce monodisperse particles in the diameter range 0.8 - 12 µm,  
340 starting from both liquid and solid materials. The MISG is used to produce soot particles from the  
341 controlled combustion of different gaseous fuels (Vernocchi et. Al. 2022).

342 Three nebulizers, designed for bioaerosol applications, are also available: the Collison nebulizer,  
343 the Blaustein Atomizing Modules (BLAM), and the Sparging Liquid Aerosol Generator (SLAG),  
344 all manufactured and distributed by CH TECHNOLOGIES Inc. The performances of the three  
345 nebulizers in connection to the injection of viable bacteria in the chamber have been previously  
346 investigated and described in (Danelli et al., 2021).

347 Bacteria injected inside ChAMBRé can be collected by different methods. All the methods  
348 described below allow to perform offline analyses. A cylindrical horizontal volume is connected  
349 to the chamber by an ISO-KF250 pneumatic valve; this volume can be alternatively opened or  
350 closed without perturbing the inner atmosphere thanks to another ISO-KF250 pneumatic valve.  
351 Inside the cylinder, there is a sliding tray that can be inserted in ChAMBRé by an external manual

352 control, to minimize the risk of contamination. The tray can host up to six Petri dishes (diameter  
353 10 cm, each) to collect bacteria (or in general BPA) directly by gravitational settling. In addition,  
354 bacteria can be collected on solid medium (i.e., Petri dishes filled with culture medium) by the  
355 active sampling by an Andersen impactor (Single Stage Andersen Cascade Impactor, TISCH  
356 Environmental) working at a fixed air flow of 28.3 lpm, supplied by a dedicated pump. The  
357 impactor is connected to the chamber by ISO-K flanges. Moreover, bioaerosol can be collected  
358 through liquid impinger, (Flow Impinger, Aquaria srl), filled with 20 ml of sterile liquid solution,  
359 . Such a device can be easily connected to the chamber volume through the ISO-K flanges.  
360 Impinger operates at a constant airflow of 12.5 lpm (e.g., by a low-capacity pump: Model LCP5,  
361 Copley Scientific). Finally, aerosol suspended in the chamber can be also collected on filters (i.e.,  
362 quartz fibre, PTFE, cellulose). Sampling is managed by a low-volume particulate matter sampler,  
363 setting the air flow in the range 10 – 50 lpm.

364

### 365 *2.3. Equipment to manipulate bioaerosol*

366 A biological laboratory with specific instrumentation for isolating and maintaining bacterial cells  
367 culture is part of the ChAMBRé facility:

- 368 • Biosafety cabinet, and laminar flow hood, Miniflow Linear blue air Aquaria, (Milano,  
369 Italy). It is used to provide a contamination-free working environment for the workers. A  
370 laminar flow filters the air and traps dust particles and microbes for providing a sterile  
371 working environment in the stainless-steel cabinet. The hood is equipped with HEPA filter  
372 and an UV-light lamp allows the sterilization of the illuminated surfaces inside the hood.
- 373 • Centrifuge MPW-352 MPW MED Instruments (Warsaw, Poland) used to separate particles  
374 from a homogeneous solution through rotational movement and centrifugal acceleration,  
375 causing sedimentation of its components. The MPW-352 has a swinging-bucket rotor that  
376 swings out when centripetal force is applied and holds the pellet at an approximate 90°  
377 angle relative to the angle of rotation.
- 378 • Spectrophotometer Shimadzu 1900, designed for liquid samples, is a double-beam UV-Vis  
379 Shimadzu Corporation, Japan. This instrument measures intensity as a function of light  
380 source wavelength. For each wavelength of light passing through the spectrometer, the  
381 intensity of the light passing through the sample cell is measured. The biological

382 applications include measurement of substance concentration such as protein, DNA or  
383 RNA, growth of bacterial cells, and enzymatic reactions.

384 • Shaker incubator, designed for liquid samples, with orbital rotation movement SKI 4  
385 ARGOLAB, Carpi MO – Italy. It provides a controlled environment for samples to grow  
386 and develop while also providing mechanical agitation to mimic the natural movement of  
387 cells in their environment. Shaking can be used to promote the growth and development of  
388 cells and microorganisms to increase the oxygen supply to the cells. The oxygen is an  
389 important factor that can affect the growth and metabolism of cells. By shaking the culture,  
390 it is possible to increase the oxygen supply to the cells by increasing the diffusion of oxygen  
391 into the media.

392 Quantum Tx microbial cell counter Logos Biosystems, South Korea. This automated cell counter  
393 can detect individual bacterial cells in a liquid sample. The instrument provides counting of the  
394 total number of cells in the suspension using fluorescent probe. It captures images of (10-fields)  
395 fluorescence-stained cells. The optimal concentration range of count is  $5 \times 10^5 - 5 \times 10^8$  cells ml<sup>-1</sup>  
396 and the size range of the count cells is between 0.3 and 50  $\mu\text{m}$ . To evaluate the uncertainty on  
397 the bacteria count (QT x TOT), we repeated the measurement on the same sample 10 times, and  
398 we found a results repeatability of 5%. This uncertainty is much higher than the statistical error of  
399 total counting (assuming the Poisson statistic), and, for this reason, we adopted a 5% uncertainty  
400 to all Quantum Tx counts. The sample is prepared from the bacterial suspension in physiological  
401 solution immediately before injection; for counting the total number of cells, three different  
402 solutions to 10  $\mu\text{l}$  of the initial suspension are added: *Total Cell Staining Dye*, *Total Cell Staining*  
403 *Enhancer* and *Loading Buffer I*. The first added is the *Total Cell Staining Dye*, a membrane-  
404 permeable fluorescent dye, which is capable of binding to nucleic acids in viable and non-viable  
405 cells and allows the detection of Gram-positive and Gram-negative bacteria. This probe has an  
406 excitation wavelength of  $\lambda = 484$  nm, and it emits  $\lambda = 504$  nm. The second solution used is the  
407 *Total Cell Staining Enhancer* to guarantee a better cells penetration by the probe and to obtain a  
408 uniform background during the images acquisition by Quantum Tx. The sample must be incubated  
409 in the dark at 37°C for about 30 minutes to favor the penetration of the fluorescent dye into the  
410 cells. Finally, the *Loading Buffer I* is added and used to uniform the distribution and the  
411 sedimentation of bacterial cells in the counting stands. The slide, after being centrifuged at 300  
412 RCF for 10 minutes, is inserted in the specific support in the counter and then illuminated with a



413 lamp at  $\lambda = 470$  nm with a bandpass of 30 nm. The light power can be set to nine levels of intensity  
414 (labelled from 1 to 9): in our experiments, the best results are obtained selecting the intensity of 5  
415 for counting total cells.

### 416 2.3.1 Bacteria cultivation, injection, monitoring and experiments in ChAMBRé

417 The bacteria strain so far used to perform experiments at ChAMBRé is *Escherichia coli* (ATCC®  
418 25922™), Gram-negative, purchased by Thermo Scientific™ Culti-Loops™. *E. coli* is rod-shaped,  
419 about 1–2  $\mu\text{m}$  long and about 0.25  $\mu\text{m}$  in diameter (Jang et al., 2017). It is a common inhabitant of  
420 the gastrointestinal apparatus of warm-blooded animals, including humans. This strain is a non-  
421 pathogen proxies of typical atmospheric bacteria, extensively used as model organisms in  
422 microbiology and molecular biology fundamental and applied studies (Lee et al., 2002; Lee and  
423 Kim, 2003).

424 The first step of our procedure was to determine the growth curve of *E. coli* by recording the optical  
425 density (OD) at  $\lambda = 600$  nm ( $\text{OD}_{600\text{nm}}$ ) at specific time intervals during the population's evolution  
426 and measuring the bacteria total concentration by the Quantum Tx and the bacteria viable  
427 concentration by standard dilution plating, as detailed in the Supplement S4.

428 To describe the growth curve of *E. coli* as a function of nutrient depletion, we followed the logistic  
429 function model that has been shown to return the best fit for modeling bacteria growth (Annadurai  
430 et al., 2000, Wachenheim et al., 2003, Akin et al., 2020). The logistic equation is written as:

431

$$432 \quad y(t) = \frac{y_0}{1 + e^{-b(t-t_0)}} \quad (1)$$

433

434 where  $y$  indicates the bacteria concentration in the solution,  $y_0$  is the saturation value,  $b$  is the  
435 maximum specific growth rate and  $t_0$  is the time at the inflection point.

436 We followed the growth of *E. coli* in suspension culture for about 8 hours from lag phase to  
437 horizontal asymptote and the values of reduced chi-squared, ( $\chi^2$ ),  $y_0$ ,  $b$  and  $t_0$  of the logistic fit for  
438  $\text{OD}_{600\text{nm}}$ , QTx TOT and CFU  $\text{ml}^{-1}$  are reported in Table 1.

439

440

441

442

443

**Table 1:**  $\chi^2$ ,  $y_0$ ,  $b$  and  $t_0$  of the logistic fit for OD<sub>600nm</sub>, QTx TOT and CFU ml<sup>-1</sup>.

Logistic 3 parameters	OD <sub>600nm</sub>	QTx TOT (# ml <sup>-1</sup> )	CFU ml <sup>-1</sup>
$\chi^2$	1.04	1.17	1.17
$y_0$	$1.35 \pm 0.01$	$(212 \pm 8) \times 10^7$	$(211 \pm 6) \times 10^7$
$b$ (min <sup>-1</sup> )	$(3.3 \pm 0.1) \times 10^{-2}$	$(3.4 \pm 0.5) \times 10^{-2}$	$(5.2 \pm 0.4) \times 10^{-2}$
$t_0$ (min)	$128 \pm 1$	$145 \pm 5$	$151 \pm 2$

444

445 The  $b$  values of OD<sub>600nm</sub> and QTx TOT are compatible within their uncertainties, and this result is  
 446 expected since the OD<sub>600nm</sub> is an indirect measurement of the total concentration of cells in  
 447 suspension. The grow rate of CFU ml<sup>-1</sup> is faster and the corresponding doubling time (about 19  
 448 minutes) is compatible with the value reported in the literature (Son et al., 2021).

449 To prepare the inoculum for the chamber experiments, the *E. coli* is grown in 30 ml of fresh TSB  
 450 (Tryptic Soy Broth) nonselective medium, in a shaking incubator at 37 °C and 200 rpm and its  
 451 growth is followed by checking the OD<sub>600nm</sub> value until the mid-exponential phase. When OD<sub>600nm</sub>  
 452 ~ 0.5, 20 ml of this liquid preparation is centrifuged at 3000 rpm for 10 min. Afterward, the bacteria  
 453 pellet, separated by supernatant, is resuspended in 20 ml of sterile physiological solution (NaCl 0.9  
 454 % w/v) to prepare a suspension of approximately 10<sup>8</sup> CFU ml<sup>-1</sup>, as verified by standard dilution  
 455 plating. To retrieve the bacterial concentration, the average of CFU counting on agar plates and  
 456 the uncertainty are calculated following the metric described in S4.

457 For the experiments performed at ChAMBRé, the typical bacterial concentration in the inoculum  
 458 is 10<sup>7</sup> CFU ml<sup>-1</sup>: to reach this concentration, a further dilution step is needed (i.e., typically 1:10  
 459 or 1:5) before the injection (see Massabò et al., 2018 for details).

460 The concentration of the solution to be injected inside ChAMBRé is also controlled in terms of  
 461 total cells ml<sup>-1</sup> by Quantum Tx Microbial Cell Counter. The sample is prepared from the bacterial  
 462 suspension in physiological solution. In each single analysis, Quantum Tx acquires 10 visual fields  
 463 of the slide's counting chamber, which correspond to an approx. volume of 0.09 µl, to retrieve the  
 464 bacterial count. To evaluate if the exposure of Quantum Tx lamp degrades the fluorescent probe  
 465 (photobleaching) of total cells, we repeated the total cell counts inserting and ejecting 10 times the  
 466 same sample: the total count probe didn't show a particular sensitivity to the exposure to the  
 467 Quantum Tx lamp, and the coefficient of variation turned out to be less than 5%. Further details  
 468 on the use of Quantum Tx counter are given in Supplement S5.

469 The bacteria suspension, properly diluted, is injected into the chamber volume mainly by using the  
470 Sparging Liquid Aerosol Generator, SLAG, which ensured the better reproducibility in earlier tests  
471 (Danelli et al., 2021). The injection phase typically lasts 5 minutes. Injection air flow and duration  
472 are automatically controlled by a Mass Flow Controller (Bronkhorst, model F201C-FA) managed  
473 via SCADA. In this way, 2 ml of bacterial suspension are nebulized inside ChAMBRe.

474 Experiments with *E. coli* have been performed by active sampling via the Andersen impactor:  
475 sampling time was progressively increased after the injection to collect a suitable number of CFUs.  
476 Sampling time during *E. coli* experiments are summarized in Table S2 in Supplement S6.

477 After the experiments in the simulation chamber, the plates sampled are incubated at 37 °C for 24  
478 h. The CFUs are then counted and, in the experiments conducted by active sampling, the CFU cm<sup>-3</sup>  
479 are calculated.

480 The possible correlation between bacteria viability and air quality can be investigated in terms of  
481 change in bacteria viability due to the exposure to atmospheric pollutants. Effects on bacteria  
482 viability are compared in relation to “baseline experiments”. In a baseline experiment, the viability  
483 of airborne bacteria is measured at atmospheric pressure, with temperatures around 20°C and with  
484 relative humidity around 60%: such values have been chosen to reproduce an environment suitable  
485 for the survival of bacteria (Dunklin, 1948; Cox, 1966; Benbough, 1967). During baseline  
486 experiments, the bacteria's viability depended on their characteristics and experimental procedures  
487 only. The baseline was assessed both in “dark” (solar simulator off) and “light” (solar simulator  
488 on) conditions. With “light” condition, the Solar Simulator was used with the AM1.5 filter  
489 mounted (see 2.1) to reduce the UV radiation; several experiments were replicated with the Solar  
490 Simulator lamp intensity set at 105% and 80% of the nominal value (i.e., the maximum and  
491 minimum intensity level which guarantees stability without using neutral filters). Baseline  
492 experiments, see Section 3, were particularly important also to assess the reproducibility and hence  
493 the sensitivity of the whole procedure.

494 The baseline assessment was followed by a set of exploratory experiments with *E. coli* exposed to  
495 selected pollutants. We measured the possible bacterial viability changes due to the exposure to  
496 atmospheric conditions typically met in polluted urban areas. So far, *E. coli* was exposed to  
497 different concentrations of NO and NO<sub>2</sub>, two of the most common pollutants emitted by vehicular  
498 and ship traffics (Seinfeld and Pandis, 1998; Monks et al., 2009; Pöschl and Shiraiwa, 2015).

499

### 3. Results

The experiments performed to investigate the possible effects on bacteria viability due to the exposure to atmospheric pollutants, were conducted by following the same procedure adopted to assess the baseline and introducing inside ChAMBRe the specific pollutant. During gas pollutant experiments, NO or NO<sub>2</sub> concentration was kept constant thanks to the feedback control system described in 2.1.3.

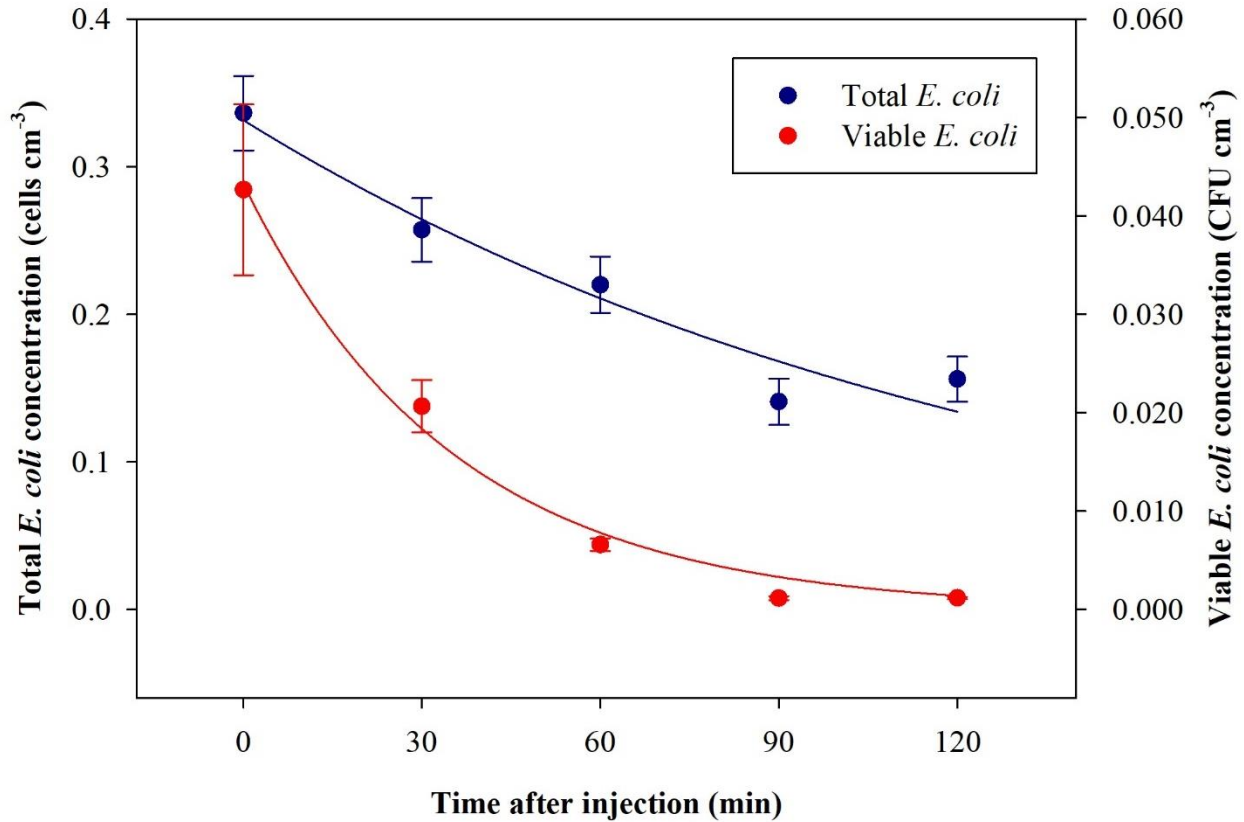
#### 3.1 Baseline experiments with *E. coli* in dark conditions.

*E. coli* behavior in a set of eight replicated experiments, led from separate cultures, was first determined in dark conditions. The average total concentration and standard deviation of *E. coli* inside the chamber at  $t = 0$  (three minutes after the conclusion of the injection to allow proper mixing/homogenization inside the ChAMBRe volume) was  $(0.34 \pm 0.08)$  cells  $\text{cm}^{-3}$ , as measured by the WIBS; the average viable concentration and standard deviation, determined by the Andersen impactor sampling at  $t = 0$  was  $(0.04 \pm 0.02)$  cells  $\text{cm}^{-3}$ . The viable concentration at  $t = 0$  was obtained by measuring the CFUs on three petri consecutively sampled; the coefficient of variation on the CFUs collected on the three petri, resulted equal to 12%.

The average ratio and standard deviation of viable:total (V:T in the following) bacteria concentration inside ChAMBRe, at  $t = 0$  turned out to be  $V:T = (0.13 \pm 0.07)$ . The total and viable bacteria concentration values measured inside ChAMBRe depended on the V:T ratio in the inoculum to be injected (biological effects between each bacteria culture) and on the aerosolization process affecting the bacteria viability. The bacteria viable concentration in the inoculum was determined via standard dilution plating while the bacteria total concentration was calculated by the Quantum Tx. During baseline experiments, the V:T ratio of the inoculum ranged between  $0.25 \pm 0.03$  and  $0.50 \pm 0.06$ . Time-trends of the averaged total and viable concentration of the bacteria, nebulized inside ChAMBRe, are shown in Figure 6. Bacteria lifetime in ChAMBRe can be calculated by fitting the data of each experiment with an exponential function as:

$$C(t) = C_0 e^{-\frac{t}{\tau}} \quad (2)$$

where  $C_0$  is the total or viable concentration of *E. coli* just after the injection ( $t = 0$ ) and  $\tau$  is the total or viable bacteria lifetime, respectively. In table 2, the average and standard deviation of  $C_0$  and  $\tau$  for the *E. coli* total and viable concentration of eight experiments are reported.



531

532 **Figure 6:** Time-trend of *E. coli* average bacteria total (blue) and viable (red) concentration inside ChAMBRE  
 533 obtained by eight repetitions of baseline experiments.

534

535 **Table 2:**  $C_0$  and  $\tau$  (average  $\pm$  std deviation) of the exponential fit for total and viable concentration of *E. coli*.

Exponential function	Total <i>E. coli</i>	Viable <i>E. coli</i>
$C_0$	$(0.33 \pm 0.08)$ cells cm <sup>-3</sup>	$(0.04 \pm 0.02)$ CFU cm <sup>-3</sup>
$\tau$ (min)	$153 \pm 22$	$32 \pm 5$

536

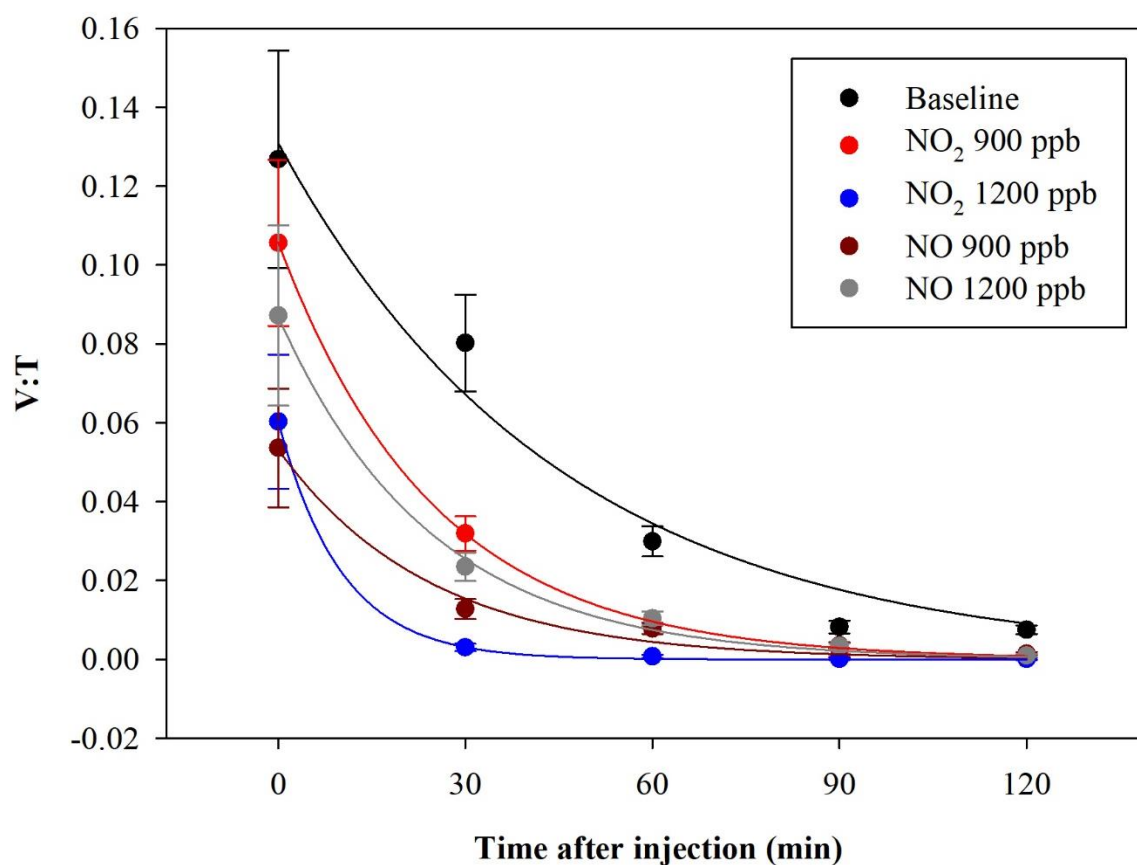
537 The total *E. coli* averaged lifetime is about 153 minutes; this value agrees with data reported in  
 538 (Massabò et al., 2018) for generic aerosols: particles in the same size range of *E. coli* (1-2  $\mu\text{m}$ ) and  
 539  $\tau=2$ -3 hours. The viable *E. coli* averaged lifetime is about 32 minutes, lower than the aerodynamic  
 540 lifetime, this indicating the difficulty of this microorganism to survive in the atmospheric medium.

### 541 3.2 Experiments with *E. coli* and NO<sub>x</sub> in dark conditions.

542 A preliminary check was performed exposing the *E. coli* to O<sub>3</sub>, which is recognized to be a strong  
 543 antimicrobial agent (Kim et al., 1999; Thanomsub et al., 2002; Giuliani et al., 2018), hence the

544 expected result was a complete viability loss. The exposure of bacteria to O<sub>3</sub> (concentration > 1000  
545 ppb) resulted in a complete cell mortality, as expected. The initial condition immediately after the  
546 injection was V:T = (0.03 ± 0.01) and no CFUs were collected in any of the following samplings  
547 (starting 30 minutes after the injection).

548 In another experiment, bacteria were exposed to NO<sub>2</sub> and NO concentrations, 900 and 1200 ppb  
549 for both the pollutants. The exposure of bacteria to such pollutants showed a V:T reduction. The  
550 average results, obtained in a set of eight experiments, led from separate cultures, are shown in  
551 Figure 7.



552  
553 **Figure 7:** Time-trend of the V:T ratio for *E. coli* in baseline (black) and in the experiments with ChAMBR<sub>e</sub> maintained  
554 at a constant concentration of: NO<sub>2</sub> (900 ppb red and 1200 ppb blue) and NO (900 ppb dark red and 1200 ppb gray).

555 The quantitative reduction in the *E. coli* lifetime, due to the exposure to pollutants, can be evaluated  
556 considering the V:T ratio and fitting the data with an exponential curve, as previously described;  
557 the results are shown in Table 3.

558 **Table 3:** Initial values and  $\tau$  (average and std deviation) of the exponential fit for V:T ratio of *E. coli* at different  
 559 pollutants concentrations.

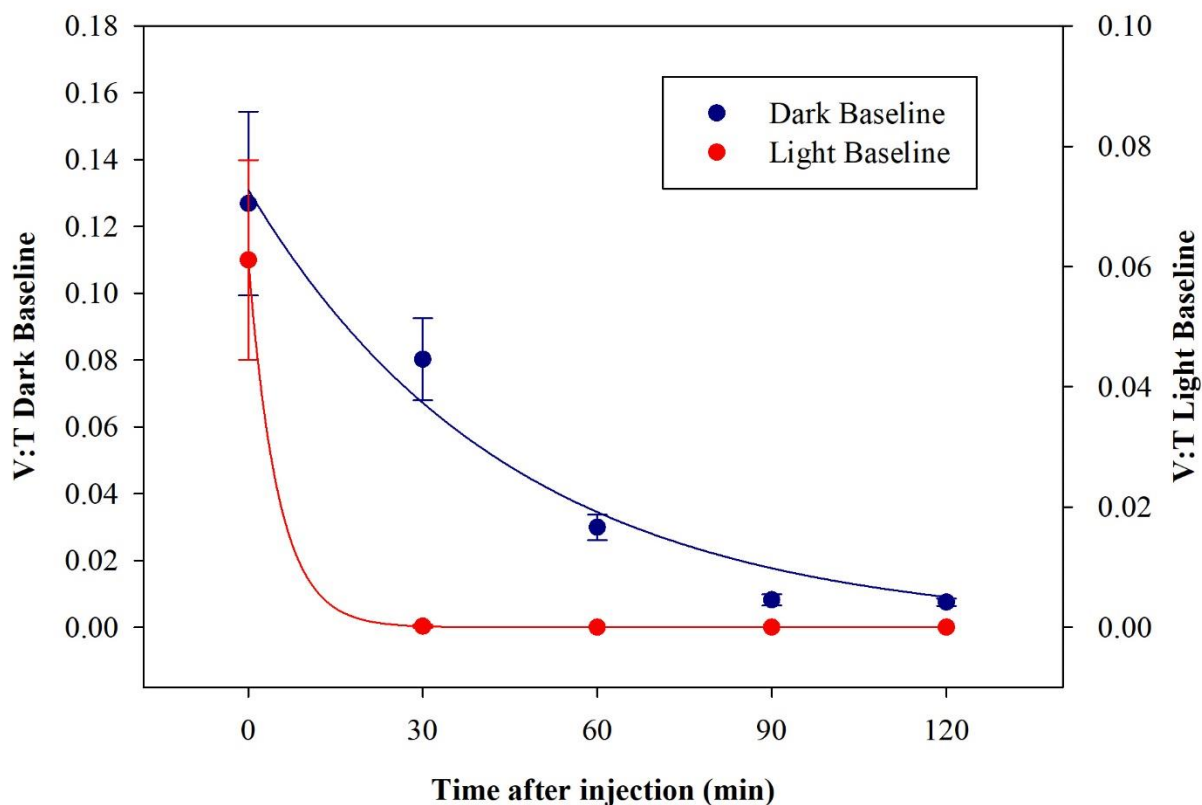
Exponential function	(V:T t = 0)	$\tau$ (min)	experiments #
Baseline	$0.13 \pm 0.07$	$40 \pm 5$	8
NO <sub>2</sub> 900 ppb	$0.11 \pm 0.02$	$25 \pm 2$	2
NO <sub>2</sub> 1200 ppb	$0.06 \pm 0.02$	$11 \pm 2$	2
NO 900 ppb	$0.05 \pm 0.01$	$26 \pm 3$	2
NO 1200 ppb	$0.10 \pm 0.02$	$25 \pm 4$	2

560  
 561 *E. coli* averaged lifetime in baseline experiments, calculated on the V:T ratio, turned out to be  
 562 about 40 min. The exposure of *E. coli* to NO<sub>2</sub> reduced the lifetime to about 25 and 11 min with a  
 563 concentration of 900 ppb and 1200 ppb respectively. The exposure to 900 ppb and 1200 ppb of  
 564 NO decreased bacteria lifetime to 26 and 25 min, respectively and the values are similar to the  
 565 value obtained with the lowest NO<sub>2</sub> concentration. The increase of the NO concentration did not  
 566 correspond to a decrease in the *E. coli* viability, as observed with NO<sub>2</sub>: these results suggest a  
 567 greater toxic effect of NO<sub>2</sub> than of NO on *E. coli*. The literature of a comparison of the toxic effects  
 568 of NO and NO<sub>2</sub> on *E. coli* is poor. Some research articles have demonstrated negative effects of  
 569 these two gases on bacterial strains: Kosaka et al., 1986 found a decrease in *E. coli* viability with  
 570 increasing NO<sub>2</sub> concentration. Janvier et al., 2020 highlighted a significant adverse effect of NO<sub>2</sub>  
 571 on some commensal skin bacterial strains. Mancinelli and McKay, 1983 found that a low  
 572 concentration of NO is bacteriostatic for some organisms but not for others. It is worth noting that  
 573 NO has a strong antimicrobial property, being an endogenously produced molecule that is critical  
 574 for critical infection defence (Fang, 1997), although some bacteria are able to escape this NO  
 575 action (Privett et al., 2012).

576  
 577 *3.2 Experiments with E. coli and Solar Simulator.*

578 *E. coli* behavior when exposed to light was determined in a set of dedicated baseline experiments.  
 579 No significant differences in results appeared changing the intensity of the Solar Simulator  
 580 operated with the AM1.5G filter and the data with a Solar Simulator intensity of 100% are here  
 581 reported. After the injection, the average total concentration of *E. coli* reached inside the chamber

582 was  $(0.30 \pm 0.03)$  cells  $\text{cm}^{-3}$ , compatible with the dark baseline; while the average viable  
583 concentration was  $(0.019 \pm 0.005)$  cells  $\text{cm}^{-3}$ , lower than what obtained in dark experiments. The  
584 consequent V:T ratio was  $(0.06 \pm 0.02)$ . The viable concentration collapses quickly, reaching zero  
585 after 30 minutes. The comparison between V:T ratio obtained for dark and light baseline is shown  
586 in Figure 8.



587  
588 **Figure 8:** Time-trend of the V:T ratio for *E. coli* in the dark baseline (dark blue) and light baseline (red) experiments.

589  
590 These results indicate a significant decrease in bacteria viability due to their exposure to solar  
591 radiation. The behavior, here evaluated in atmospheric environment, agrees with observation in  
592 water environments reported in several works (Whitman et al., 2004; Jozić et al., 2014; Tiwari et  
593 al., 2022); the solar radiation is indicated as an abiotic factor with the negative effect of bringing  
594 some bacteria strains, among which *E. coli*, into a temporary inactivation/non-cultivable state.

595  
596  
597



#### 598 4. Discussion, conclusion, and perspectives

599 The main result presented in this work is the assessment of a multi-step and well controlled  
600 protocol to perform experiments on the impact of air quality on bacteria viability by an atmospheric  
601 simulation chamber, ChAMBRé in this case. Even if the chamber configuration is still in progress  
602 and several new equipment will be deployed at ChAMBRé in the near future, the present set-up  
603 opens the possibility of systematic studies. The average  $\tau$  of the V:T ratio of eight baseline  
604 experiments was 40 min with a standard deviation of 5 min; the coefficient of variation of 13%  
605 corresponds to the experimental sensitivity to changes in *E. coli* viability due to exposure to  
606 pollutants and/or other relevant parameters. The baseline reference must be experimentally  
607 determined for each bacteria strain and efforts are planned for repeating the observation with  
608 *Bacillus subtilis*, *Bacillus spizizenii* and *Pseudomonas fluorescens* in the near future. It is worthy  
609 to note that the experimental protocol returns the lifetime of total and viable bacteria injected in  
610 the chamber. The figure for total bacteria corresponds to the aerodynamic behavior of aerosol of  
611 diameter around 1  $\mu\text{m}$ , already reported in (Massabò et al., 2008) while the lifetime of viable  
612 bacteria is much shorter (about half an hour) due to the difficulty of this microorganism to survive  
613 in the atmospheric medium. Such shorter lifetime posed clear constraints on the first experiments  
614 with exposure of *E. coli* to  $\text{NO}_x$  inside ChAMBRé. A time window of two hours after the bacteria  
615 injection was considered to observe the behavior of *E. coli* viability and it was possible to quantify  
616 a lifetime reduction, in dark conditions, clearly related to NO and  $\text{NO}_2$  concentration inside  
617 ChAMBRé. These findings pave the road to systematic studies including other bacteria strains and  
618 pollutant species. With the *E. coli* exposed to the light produced by the Solar Simulator operated  
619 with the AM1.5 filter, the viability resulted very short even in the baseline conditions and therefore  
620 no further experiment with pollutants was performed. With other bacterial strains, the impact of  
621 light on viability will have to be reinvestigated.

622 It is well known in the literature that the viable but non-culturable condition (VBNC) is a survival  
623 strategy of many bacteria in the environment in response to adverse environmental conditions (e.g.,  
624 solar radiation). There is a growing scientific interest in studying VBNC cells, including to  
625 understand novel public health implications of VBNC cells. In our simulated experiments, we are  
626 investigating alternative methods to detect bacterial viability and VBNC state, such as “live and  
627 dead staining” by fluorescence microscopy. This assay can be used to monitor the viability of  
628 bacterial populations as a function of cell membrane integrity using different fluorescent dyes.

629 Further experiments with “flow cytometry” could certainly be more beneficial not only to  
630 enumerate live and dead bacteria, but also to evaluate the health and viability of bacterial cells by  
631 determining the activity of bacterial oxidases and reductases.

632

## 633 **5. Acknowledgments**

634 We are indebted to the personnel of the mechanical workshop of the INFN division of Genoa for  
635 the continuous support in the development of the ChAMBRé structure. The development of the  
636 chamber and the deployment of the equipment was supported by several European and Italian  
637 projects/grants: EUROCHAMP2020 (H2020: Infrastructure Activity under grant agreement No  
638 730997); PON per-ACTRIS-IT (MUR-IT: PON project PIR\_00015 “Per ACTRIS IT”); BLUE-  
639 LAB NET (F.E.S.R. - FONDO EUROPEO DI SVILUPPO REGIONALE Azione POR, Regione  
640 Liguria, IT); ATMO-ACCESS (H2020: Infrastructure Activity under grant agreement No  
641 101008004); NextGenerationEU PNRR-ITINERIS (Italian Integrated Environmental Research  
642 Infrastructures System). The publication has been funded by EU - Next Generation EU Mission 4  
643 “Education and Research” - Component 2: “From research to business” - Investment 3.1: “Fund  
644 for the realisation of an integrated system of research and innovation infrastructures” - Project  
645 IR0000032 – ITINERIS - Italian Integrated Environmental Research Infrastructures System - CUP  
646 B53C22002150006. The authors acknowledge the Research Infrastructures participating in the  
647 ITINERIS project with their Italian nodes: ACTRIS, ANAEE, ATLaS, CeTRA, DANUBIUS,  
648 DISSCO, e-LTER, ECORD, EMPHASIS, EMSO, EUFAR, Euro-Argo, EuroFleets, Geoscience,  
649 IBISBA, ICOS, JERICO, LIFEWATCH, LNS, N/R Laura Bassi, SIOS, SMINO.

650

## 651 **6. References**

652 Akin, E., Pelen, N. N., Tiryaki, I. U., Yalcin, F.: Parameter identification for gompertz and logistic  
653 dynamic equations, PLoS ONE 15(4): e0230582, <https://doi.org/10.1371/journal.pone.0230582>,  
654 2020.

655 Amato, P., Demeer, F., Melaouhi, A., Fontanella, S., Martin-Biesse, A.-S., Sancelme, M., Laj, P.,  
656 Delort, A.-M.: A fate for organic acids, formaldehyde and methanol in cloud water: their  
657 biotransformation by micro-organisms, *Atmospheric Chem. Phys.* 7, 4159–4169, 2007.

658 Amato, P., Joly, M., Schaupp, C., Attard, E., Möhler, O., Morris, C.E., Brunet, Y., Delort, A.-M.:  
659 Survival and ice nucleation activity of bacteria as aerosols in a cloud simulation chamber,  
660 *Atmospheric Chem. Phys.* 15, 6455–6465. <https://doi.org/10.5194/acp-15-6455-2015>, 2015.

661 Amato, P., Mathonat, F., Nuñez Lopez, L., Péguilhan, R., Bourhane, Z., Rossi, F., Vyskocil, J.,  
662 Joly, M., and Ervens, B.: The aeromicrobiome: the selective and dynamic outer-layer of the Earth's  
663 microbiome, *Frontiers in Microbiology*, 14, <https://doi.org/10.3389/fmicb.2023.1186847>, 2023

664 Annadurai, G., Rajesh Babu, S., Srinivasamoorthy, V. R.: Development of mathematical models  
665 (Logistic, Gompertz and Richards models) describing the growth pattern of *Pseudomonas putida*  
666 (NICM 2174), *Bioprocess Engineering*, 23(6), 607-612, <https://doi.org/10.1007/s004490000209>,  
667 2000.

668 Ariya, P.A., Amyot, M.: New Directions: The role of bioaerosols in atmospheric chemistry and  
669 physics, *Atmos. Environ.* 38, 1231–1232, <https://doi.org/10.1016/j.atmosenv.2003.12.006>, 2004.

670

671 Bauer, H., Giebl, H., Hitzemberger, R., Kasper-Giebl, A., Reischl, G., Zibuschka, F., Puxbaum, H.:  
672 Airborne bacteria as cloud condensation nuclei, *Journal of Geophysical Research*, vol. 108, no.  
673 D21, 4658, doi:10.1029/2003JD003545, 2003.

674 Benbough, J. E.: Death Mechanisms in Airborne *Escherichia coli*, *J. Gen. Microbiol.* 47, 325–  
675 333, <https://doi.org/10.1099/00221287-47-3-325>, 1967.

676 Bolashikov, Z. D., Melikov, A.K.: Methods for air cleaning and protection of building occupants  
677 from airborne pathogens, *Build Environ.* 44(7):1378-1385. doi: 10.1016/j.buildenv.2008.09.001,  
678 2009.

679 Brotto, P., Repetto, B., Formenti, P., Pangui, E., Livet, A., Bousserhine, N., Martini, I., Varnier,  
680 O., Doussin, J.F., Prati, P.: Use of an atmospheric simulation chamber for bioaerosol investigation:  
681 a feasibility study, *Aerobiologia* 31, 445–455, <https://doi.org/10.1007/s10453-015-9378-2>, 2015.

682 Bundke, U., Reimann, B., Nillius, B., Jaenicke, R., Bingemer, H.: Development of a Bioaerosol  
683 single particle detector (BIO IN) for the Fast Ice Nucleus CHamber FINCH, *Atmos. Meas. Tech.*,  
684 3, 263–271, <https://doi.org/10.5194/amt-3-263-2010>, 2010.

685 Burrows, S. M., Butler, T., Jöckel, P., Tost, H., Kerkweg, A., Pöschl, U., Lawrence, M.G.: Bacteria  
686 in the global atmosphere – Part 2: Modeling of emissions and transport between different  
687 ecosystems, *Atmospheric Chem. Phys.* 9, 9281–9297. <https://doi.org/10.5194/acp-9-9281-2009>,  
688 2009.

689 Chou, C., Stetzer, O., Weingartner, E., Jurányi, Z., Kanji, Z. A., Lohmann, U.: Ice nuclei properties  
690 within a Saharan dust event at the Jungfraujoch in the Swiss Alps, *Atmos. Chem. Phys.*, 11, 4725–  
691 4738, <https://doi.org/10.5194/acp-11-4725-2011>, 2011.

692 CID, Commission Implementing Decision (EU) 2023/900, “Setting up the Aerosol, Clouds and  
693 Trace Gases Research Infrastructure (ACTRIS ERIC)” Official Journal of the European Union  
694 L115/15, 03/05/2023.

695 Cox, C.S.: The Survival of *Escherichia coli* sprayed into Air and into Nitrogen from Distilled  
696 Water and from Solutions of Protecting Agents, as a Function of Relative Humidity, *J. Gen.*  
697 *Microbiol.* 43, 383–399, <https://doi.org/10.1099/00221287-43-3-383>, 1966.

698 Danelli, S., Brunoldi, M., Massabò, D., Parodi, F., Vernocchi, V., Prati, P.: Comparative  
699 characterization of the performance of bio-aerosol nebulizers in connection with atmospheric  
700 simulation chambers. *Atmos. Meas. Tech.*, 14, 4461–4470, [https://doi.org/10.5194/amt-14-4461-](https://doi.org/10.5194/amt-14-4461-2021)  
701 2021, 2021.

702 Deguillaume, L., Leriche, M., Amato, P., Ariya, P.A., Delort, A.-M., Pöschl, U., Chaumerliac, N.,  
703 Bauer, H., Flossmann, A.I., Morris, C.E.: Microbiology and atmospheric processes: chemical  
704 interactions of primary biological aerosols, *Biogeosciences* 5, 1073–1084,  
705 <https://doi.org/10.5194/bg-5-1073-2008>, 2008.

706 Delort, A. M., Väitilingom, M., Amato, P., Sancelme, M., Parazols, M., Mailhot, G., Laj, P.,  
707 Deguillaume, L.: A short overview of the microbial population in clouds: Potential roles in  
708 atmospheric chemistry and nucleation processes, *Atmospheric Research*, Volume 98, Issues 2–4,  
709 Pages 249-260, <https://doi.org/10.1016/j.atmosres.2010.07.004>, 2010.

710 Després, V. R., Huffman, J. A., Burrows, S. M., Hoose, C., Safatov, A. S., Buryak, G., Fröhlich-  
711 Nowoisky, J., Elbert, W., Andreae, M.O., Pöschl, U., Jaenicke, R.: Primary biological aerosol  
712 particles in the atmosphere: a review. *Tellus B Chem. Phys. Meteorol.* 64, 15598,  
713 <https://doi.org/10.3402/tellusb.v64i0.15598>, 2012.

714 Dunklin, E. W., Puck, T. T.: The lethal effect of relative humidity on airborne bacteria. *J. Exp.*  
715 *Med.* 87, 87–101, <https://doi.org/10.1084/jem.87.2.87>, 1948.

716 Ehrlich, R., Miller, S., and Walker, R. L.: Relationship Between Atmospheric Temperature and  
717 Survival of Airborne Bacteria, *Appl Microbiol*, 19, 245–249, 1970.

718 Ervens, B. and Amato, P.: The global impact of bacterial processes on carbon mass. *Atmos. Chem.*  
719 *Phys.*, 20, 1777–1794, <https://doi.org/10.5194/acp-20-1777-2020>, 2020.

720 Fang, F. C.: Perspectives series: host/pathogen interactions. Mechanisms of nitric oxide-related  
721 antimicrobial activity, *J Clin Invest.* 99(12): 2818–2825, [https://doi.org/10.1172%2FJCI119473,](https://doi.org/10.1172%2FJCI119473.1997)  
722 [1997.](https://doi.org/10.1172%2FJCI119473.1997)

723 Fankhauser, A. M., Antonio, D. D., Krell, A. M., Alston, S. J., Banta, S., and McNeill, V. F.:  
724 Constraining the impact of bacteria on the aqueous atmospheric chemistry of small organic  
725 compounds, *ACS Earth Space Chem.*, <https://doi.org/10.1021/acsearchspacechem.9b00054>, 2019.

726 Fröhlich-Nowoisky, J., Kampf, C. J., Weber, B., Huffman, J. A., Pöhlker, C., Andreae, M. O.,  
727 Lang-Yona, N., Burrows, S. M., Gunthe, S. S., Elbert, W., Su, H., Hoor, P., Thines, E., Hoffmann,  
728 T., Després, V. R., Pöschl, U.: Bioaerosols in the Earth system: Climate, health, and ecosystem  
729 interactions. *Atmospheric Res.* 182, 346–376, <https://doi.org/10.1016/j.atmosres.2016.07.018>,  
730 2016.

731 Giuliani, G., Ricevuti, G., Galoforo, A., Franzini, M.: Microbiological aspects of ozone:  
732 bactericidal activity and antibiotic/antimicrobial resistance in bacterial strains treated with ozone.  
733 *Ozone Therapy*, 3(3), <https://doi.org/10.4081/ozone.2018.7971>, 2018.

734 Gong, J., Qi, J., E, B., Yin, Y., Gao, D.: Concentration, viability and size distribution of bacteria  
735 in atmospheric bioaerosols under different types of pollution. *Environmental Pollution* 257,  
736 113485, <https://doi.org/10.1016/j.envpol.2019.113485>, 2020.

737 Hall, B. G., Acar, H., Nandipati, A., Barlow, M.: Growth Rates Made Easy, *Mol. Biol. Evol.* 31,  
738 232–238, <https://doi.org/10.1093/molbev/mst187>, 2014.

739 Jaber, S., Lallement, A., Sancelme, M., Leremboure, M., Mailhot, G., Ervens, B., and Delort, A.-  
740 M.: Biodegradation of phenol and catechol in cloud water: comparison to chemical oxidation in  
741 the atmospheric multiphase system, *Atmospheric Chemistry and Physics*, 20, 4987–4997,  
742 <https://doi.org/10.5194/acp-20-4987-2020>, 2020.

743 Jaber, S., Joly, M., Brissy, M., Leremboure, M., Khaled, A., Ervens, B., and Delort, A.-M.: Biotic  
744 and abiotic transformation of amino acids in cloud water: experimental studies and atmospheric  
745 implications, *Biogeosciences*, 18, 1067–1080, <https://doi.org/10.5194/bg-18-1067-2021>, 2021.

746 Jang, J., Hur, H.-G., Sadowsky, M. J., Byappanahalli, M. N., Yan, T., Ishii, S.: Environmental  
747 *Escherichia coli*: ecology and public health implications-a review, *J. Appl. Microbiol.* 123, 570–  
748 581, <https://doi.org/10.1111/jam.13468>, 2017.

749 Janvier, X., Alexandre, S., Boukerb, A. M., Souak, D., Maillot, O., Barreau, M., Gouriou, F.,  
750 Grillon, C., Feuilloley, M. G. J., Groboillot, A.: Deleterious Effects of an Air Pollutant (NO<sub>2</sub>) on  
751 a Selection of Commensal Skin Bacterial Strains, Potential Contributor to Dysbiosis?, *Frontiers of*  
752 *in Microbiology*, Volume 11, Article 591839, <https://doi.org/10.3389/fmicb.2020.591839>, 2020.  
753

754 Jozić, S., Morović, M., Šolić, M., Krstulović, N., Ordulj, M.: Effect of solar radiation, temperature  
755 and salinity on the survival of two different strains of *Escherichia coli*, *Fresenius Environ. Bull.*  
756 23, 1852–1859, 2014.

757 Khaled, A., Zhang, M., Amato, P., Delort, A.-M., and Ervens, B.: Biodegradation by bacteria in  
758 clouds: an underestimated sink for some organics in the atmospheric multiphase system,  
759 *Atmospheric Chemistry and Physics*, 21, 3123–3141, <https://doi.org/10.5194/acp-21-3123-2021>,  
760 2021.

761 Krumins, V., Mainelis, G., Kerkhof, L. J., and Fennell, D. E.: Substrate-Dependent rRNA  
762 Production in an Airborne Bacterium, *Environ. Sci. Technol. Lett.*, 1, 376–381,  
763 <https://doi.org/10.1021/ez500245y>, 2014.

764 Kim, J. G., Yousef, A. E., Dave, S.: Application of Ozone for Enhancing the Microbiological  
765 Safety and Quality of Foods: A Review, *Journal of Food Protection*, 62, 9, 1071-1087,  
766 <https://doi.org/10.4315/0362-028X-62.9.1071>, 1999.

767

768 Kosaka, H., Yamamoto, H., Oda, Y., Uozumi, M.: Induction of SOS functions by nitrogen dioxide  
769 in *Escherichia coli* with different DNA-repair capacities, *Mutat Res. Aug*; 162(1):1-5, doi:  
770 10.1016/0027-5107(86)90065-5, 1986.

771 Lee, B. U., Kim, S. H., Kim, S. S.: Hygroscopic growth of *E. coli* and *B. subtilis* bioaerosols,  
772 Journal of Aerosol Science 33, 1721–1723, [https://doi.org/10.1016/S0021-8502\(02\)00114-3](https://doi.org/10.1016/S0021-8502(02)00114-3),  
773 2002.

774 Lee, B. U., Kim, S. S.: Sampling *E. coli* and *B. subtilis* bacteria bioaerosols by a new type of  
775 impactor with a cooled impaction plate, J. Aerosol Sci., 34, 1097–1100, 2003.

776 Lieberherr, G., Auderset, K., Calpini, B., Clot, B., Crouzy, B., Gysel-Beer, M., Konzelmann, T.,  
777 Manzano, J., Mihajlovic, A., Moallemi, A., O'Connor, D., Sikoparija, B., Sauvageat, E., Tummon,  
778 F., Vasilatou, K: Assessment of real-time bioaerosol particle counters using reference chamber  
779 experiments, Atmos. Meas. Tech., 14, 7693–7706, <https://doi.org/10.5194/amt-14-7693-2021>,  
780 2021.

781 Lighthart, B., Shaffer, B.T., Marthi, Ganio, L. M.: Artificial wind-gust liberation of microbial  
782 bioaerosols previously deposited on plants. Aerobiologia 9, 189–196,  
783 <https://doi.org/10.1007/BF02066261>, 1993.

784 Mancinelli, R. L. and McKay, C.P.: Effects of Nitric Oxide and Nitrogen Dioxide on Bacterial  
785 Growth, Applied and Environmental Microbiology, 198–202,  
786 <https://doi.org/10.1128/aem.46.1.198-202.1983>, 1983.

787 .

788 Martiny, J. B. H., Bohannan, B. J. M., Brown, J. H., Colwell, R. K., Fuhrman, J. A., Green, J. L.,  
789 Horner-Devine, M. C., Kane, M., Krumins, J. A., Kuske, C. R., Morin, P. J., Naeem, S., Ovreås,  
790 L., Reysenbach, A.-L., Smith, V. H., Staley, J. T.: Microbial biogeography: putting  
791 microorganisms on the map. Nat. Rev. Microbiol. 4, 102–112,  
792 <https://doi.org/10.1038/nrmicro1341>, 2006.

793 Massabò, D., Danelli, S. G., Brotto, P., Comite, A., Costa, C., Di Cesare, A., Doussin, J. F.,  
794 Ferraro, F., Formenti, P., Gatta, E., Negretti, L., Oliva, M., Parodi, F., Vezzulli, L., Prati, P.:  
795 ChAMBRé: a new atmospheric simulation chamber for aerosol modelling and bio-aerosol  
796 research, Atmos. Meas. Tech., 11, 5885–5900, <https://doi.org/10.5194/amt-11-5885-2018>, 2018.

797 Mayol, E., Jiménez, M. A., Herndl, G. J., Duarte, C. M., and Arrieta, J. M.: Resolving the  
798 abundance and air-sea fluxes of airborne microorganisms in the North Atlantic Ocean. Frontiers  
799 in Microbiology, 5, <https://doi.org/10.3389/fmicb.2014.00557>, 2014.

800 Möhler, O., DeMott, P. J., Vali, G., Levin, Z.: Microbiology and atmospheric processes: the role  
801 of biological particles in cloud physics, Biogeosciences 4, 1059–1071, [https://doi.org/10.5194/bg-](https://doi.org/10.5194/bg-4-1059-2007)  
802 4-1059-2007, 2007.

803 Monks, P. S., Granier, C., Fuzzi, S., Stohl, A., Williams, M. L., Akimoto, H., Amann, M.,  
804 Baklanov, A., Baltensperger, U., Bey, I., Blake, N., Blake, R. S., Carslaw, K., Cooper, O. R.,  
805 Dentener, F., Fowler, D., Fragkou, E., Frost, G. J., Generoso, S., Ginoux, P., Grewe, V., Guenther,  
806 A., Hansson, H. C., Henne, S., Hjorth, J., Hofzumahaus, A., Huntrieser, H., Isaksen, I. S. A.,  
807 Jenkin, M. E., Kaiser, J., Kanakidou, M., Klimont, Z., Kulmala, M., Laj, P., Lawrence, M. G., Lee,  
808 J. D., Liousse, C., Maione, M., McFiggans, G., Metzger, A., Mieville, A., Moussiopoulos, N.,

809 Orlando, J. J., O'Dowd, C. D., Palmer, P. I., Parrish, D. D., Petzold, A., Platt, U., Pöschl, U.,  
810 Prévôt, A. S. H., Reeves, C. E., Reimann, S., Rudich, Y., Sellegri, K., Steinbrecher, R., Simpson,  
811 D., ten Brink, H., Theloke, J., van der Werf, G. R., Vautard, R., Vestreng, V., Vlachokostas, Ch.,  
812 von Glasow, R.: Atmospheric composition change – global and regional air quality, *Atmos.*  
813 *Environ.* 43, 5268–5350, <https://doi.org/10.1016/j.atmosenv.2009.08.021>, 2009.

814 Moosmüller, H., Chakrabarty, R. K., Arnott, W. P.: Aerosol light absorption and its measurement:  
815 A review, *Journal of Quantitative Spectroscopy and Radiative Transfer* Volume 110, Issue 11,  
816 Pages 844–87, <https://doi.org/10.1016/j.jqsrt.2009.02.035>, 2009.

817 Morris, C. E., Georgakopoulos, D. G., Sands, D. C.: Ice nucleation active bacteria and their  
818 potential role in precipitation. *J. Phys. IV Proc.* 121, 87–103,  
819 <https://doi.org/10.1051/jp4:2004121004>, 2004.

820 Morris, C. E., Leyronas, C., Nicot, P. C.: Movement of Bioaerosols in the Atmosphere and the  
821 Consequences for Climate and Microbial Evolution, in: Colbeck, I., Lazaridis, M. (Eds.), *Aerosol*  
822 *Science: Technology and Applications*. John Wiley & Sons, Ltd, Chichester, UK, pp. 393–415,  
823 <https://doi.org/10.1002/9781118682555.ch16>, 2014.

824 Pöschl, U.: Atmospheric Aerosols: Composition, Transformation, Climate and Health Effects,  
825 *Angew. Chem. Int. Ed.* 44, 7520–7540, <https://doi.org/10.1002/anie.200501122>, 2005.

826 Pöschl, U., Shiraiwa, M.: Multiphase Chemistry at the Atmosphere–Biosphere Interface  
827 Influencing Climate and Public Health in the Anthropocene, *Chem. Rev.* 115, 4440–4475,  
828 <https://doi.org/10.1021/cr500487s>, 2015.

829 Privett, B. J., Broadnax, A. D., Bauman, S. J., Riccio, D. A., Schoenfisch, M. H.: Examination of  
830 bacterial resistance to exogenous nitric oxide, *Nitric Oxide*, Volume 26, Issue 3, Pages 169–173,  
831 <https://doi.org/10.1016/j.niox.2012.02.002>, 2012.

832 Romano, S., Di Salvo, M., Rispoli, G., Alifano, P., Perrone, M. R., Talà, A.: Airborne bacteria in  
833 the Central Mediterranean: Structure and role of meteorology and air mass transport, *Science of*  
834 *the Total Environment* 697 (2019) 134020, <https://doi.org/10.1016/j.scitotenv.2020.138899>, 2019.

835 Seinfeld, J. H., Pandis, S. N.: *Atmospheric Chemistry and Physics: From Air Pollution to Climate*  
836 *Change*, Wiley-Interscience, ISBN 10: 0471178152 ISBN 13: 9780471178156, 1998.

837 Shaffer, B.T., Lighthart, B.: Survey of Culturable Airborne Bacteria at Four Diverse Locations in  
838 Oregon: Urban, Rural, Forest, and Coastal, *Microb. Ecol.* 34, 167–177,  
839 <https://doi.org/10.1007/s002489900046>, 1997.

840 Son, M. S., Taylor R. K.: Growth and Maintenance of *Escherichia coli* Laboratory Strains, *Curr.*  
841 *Protoc.* 2021 January; 1(1): e20, <https://doi.org/10.1002/cpz1.20>, 2021.

842 Sun, J., Ariya, P.: Atmospheric organic and bio-aerosols as cloud condensation nuclei (CCN): A  
843 review, *Atmos. Environ.* 40, 795–820, <https://doi.org/10.1016/j.atmosenv.2005.05.052>, 2006.

844 Thanomsub, B., Anupunpisit, V., Chanphetch, S., Watcharachaipong, T., Poonkhum, R., and  
845 Srisukonth, C.: Effects of ozone treatment on cell growth and ultrastructural changes in bacteria,  
846 J. Gen. Appl. Microbiol., 48, 193–199, <https://doi.org/10.2323/jgam.48.193>, 2002.

847 Tiwari, A., Kauppinen, A., Räsänen, P., Salonen, J., Wessels, L., Juntunen, J., Miettinen, I. T.,  
848 Pitkänen, T.: Effects of temperature and light exposure on the decay characteristics of fecal  
849 indicators, norovirus, and Legionella in mesocosms simulating subarctic river water, Sci. Tot. Env.  
850 859, <https://doi.org/10.1016/j.scitotenv.2022.160340>, 2022.

851 Vernocchi, V., Brunoldi, M., Danelli, S. G., Parodi, F., Prati, P., Massabò, D.: Characterization of  
852 soot produced by the mini-inverted soot generator with an atmospheric simulation chamber,  
853 Atmos. Meas. Tech., 15, 2159–2175, <https://doi.org/10.5194/amt-15-2159-2022>, 2022.

854 Wachenheim, D. E., Patterson, J. A., Ladish, M. R.: Analysis of the logistic function model:  
855 derivation and applications specific to batch cultured microorganisms, Bioresource Technology  
856 Volume 86, Issue 2 Pages 157-164, [https://doi.org/10.1016/S0960-8524\(02\)00149-9](https://doi.org/10.1016/S0960-8524(02)00149-9), 2003.

857 Wagstrom, K. M., Pandis, S. N., Yarwood, G., Wilson, G. M., Morris, R. E.: Development and  
858 application of a computationally efficient particulate matter apportionment algorithm in a three-  
859 dimensional chemical transport model. Atmos. Environ. 42 (2008) 5650–5659,  
860 <https://doi.org/10.1016/j.atmosenv.2008.03.012>, 2008.

861 Wang, C.-C., Fang, G.-C., Lee, L.: Bioaerosols study in central Taiwan during summer season,  
862 Toxicol. Ind. Health 23, 133–139, <https://doi.org/10.1177/0748233707078741>, 2007.

863 Whitman, R. L., Nevers, M. B., Korinek, G.C., Byappanahalli, M.N.: Solar and temporal effects  
864 on *Escherichia coli* concentration at a Lake Michigan swimming beach, Appl Environ Microbiol.  
865 Vol 70, No. 7, <https://doi.org/10.1128/AEM.70.7.4276-4285.2004>, 2004.

866 Wright, D. N., Bailey, G. D., and Goldberg, L. J.: Effect of Temperature on Survival of Airborne  
867 Mycoplasma pneumoniae, J Bacteriol, 99, 491–495, 1969.

868 Zwietering, M. H., Jongenburger, I., Rombouts, F. M., van 't Riet, K.: Modeling of the bacterial  
869 growth curve, Appl Environ Microbiol. 1990 Jun; 56(6): 1875–1881, DOI:  
870 <https://doi.org/10.1128/aem.56.6.1875-1881.1990>, 1990.